2014

The Effect of Rainfall and Post-revolutionary Land-use Changes on Sediment Yield in Weixi Basin, Yunnan, China : New insights from multi-temporal land-use classification and radionuclide analyses

Yue Qiu
Oberlin College

The Effect of Rainfall and Post-revolutionary Land-use Changes On Sediment Yield in Weixi Basin, Yunnan, China

New insights from multi-temporal land-use classification and radionuclide analyses

Yue Qiu
Advisor: Amanda Schmidt
Oberlin College Spring 2014

Table of Contents

Abstract

This paper looks at the dynamic interphase connecting post-revolutionary politics, modern land use practices, precipitation patterns, basin slope, and sediment yield records in Weixi basin, a small mountainous watershed in Southwestern China with a total upstream area of 198 m^2. The goal is to identify what processes, climatic or not, account for the changes in local sediment yield and erosion budget. Weixi Basin has an average annual sediment yield of 175 ton/km^2 with two anomalously large peaks in 1979 and 1984. Precipitation is moderately correlated with sediment yield at interannual scale. It also affects seasonal fluctuations in sediment yield as major sediment loading events correspond to spring snowmelt and monsoon rainfall. However, there is no long-term trend in precipitation that could explain the peak in sediment yield. Land use/land cover classification shows an average of 22.8% bare land in Weixi basin, but no definitive conclusion about temporal changes could be drawn yet due to the discrepancy in imagery resolution. Short-lived radionuclide analyses show there is no correlation between upstream land use and depth of erosion, whereas slope is a moderate control for erosion depth.

Chapter 1. Deforestation and Erosion in Rural Yunnan, China

Introduction

China has a long recorded history of civilization and human manipulation of ecosystems (Frayer et al., 2013). It has few, if any, unaltered forests; many Chinese forests have been cut, used, managed, and regenerated over and over. Changes in land use, especially clearance of land for farming and grazing predates the modern era. The conflict between the traditional Chinese ideals of conservation and the desire to exploit natural resources has existed since ancient times (Menzies, 1994). Changes in land ownership and wars associated with the succession of over 30 dynasties have left China's natural resources, especially forests, seriously degraded. Trees were cut down for various reasons including clearance for farming and settlement, provision of fuel woods for domestic uses, and the supply of timbre for construction (Elvin, 2006). There was clear evidence for the shortage of timber and other environmental challenges as early as 1850 (Marks, 2012).

Despite the vast land degradation, some parts of the hills and mountains in China still had extensive forests, including Yunnan when the People's Republic of China was founded in 1949 (Marks, 2012). Yet the clearance of land has only intensified during the following half century. Deforestation, the removal of a forest followed by the conversion of land to a non-forest uses such as farms, ranches, or urban developments and dwellings, accelerated to a new speed during Mao's era (1949-mid 70's). The latest rounds of deforestation occurred during the "three great cuttings": the Great Leap Forward from 1958 to 1961, the Cultural Revolution from 1966 to 1976, and Deng's Reform Era from 1978 to 1988 (Marks, 2012). According to data from National Forest Resource Inventory (NFRI), which is conducted every five years in China, forest cover was as low as 12% in 1981 (Song and Zhang, 2010).

The negative effects of deforestation on the landscape are well established. Human activities are thought to have changed 50% of the earth, and are among the most prominent geomorphic agents to shape local and regional landscape (Hooke, 2000; Hooke et al., 2012). In addition to its contribution to global warming (Fearnside and Laurance, 2004) and decline in biodiversity (Jha and Bawa, 2006), deforestation also affects the soils and local hydrology (Sahin and Hall, 1996; Long et al., 2006). Land clearance leads to reducing soil cohesion, which in turn increases erosion rate and can result in landslides, flooding, and siltation in waterways downstream, posing a serious threat to people living nearby (IPCC, 2000). Scholars from around the world have argued that the environmental degradation along the major rivers in China is largely due to anthropogenic changes, namely the increasing rate of urbanization, deforestation and the adoption of aggressive agricultural practices since the 1950s under the influence of China's post-revolutionary policies (Shapiro, 2001, Trac et al., 2007).

Despite the lament of the loss in forest cover and its connection to rapid erosion in watersheds, there is not yet a scientific consensus on the change in sediment yield in response to upstream land uses. While Walling and Webb (1996) suggested that there should be an increasing trend in sediment yield in rivers correlated with deforestation, many found more ambivalent results (e.g. Zhang and Wen, 2004; Zhang et al., 2006). In particular, the extent of the effect of agricultural activities and land-use changes on sediment yield in Southwest China is still a puzzling case. Contradictory to what many scholars believe (e.g., Chen, 2000 and Yin and Li, 2001), some studies found that there is no systematic trend in sediment yield data despite the massive logging and deforestation from early 1960s to 1980s in some studies in Southwest China and Southeast Tibet (Lu and Higgitt, 1998, Schmidt et al., 2011).

In addition to land use/land cover, precipitation is another factor commonly associated with erosion in mountainous areas (e.g., Reiners et al., 2003). Langbein and Schumm (1958) proposed a threshold relationship between annual precipitation and sediment yield with a maximum of sediment flux at 254-355 mm of precipitation per year. They used a precipitation-runoff curve to convert known values of annual runoff to effective precipitation. The "Langbein-Schumm Rule" was, however, criticized by Wilson's (1973) paper in which he suggests that sediment yield is influenced more by non-climatic factors such as land use than precipitation. He also argues that the relationship extrapolated by Langbein and Schumm (1958) is not valid on a world-wide basis. Despite the critique on the "Langbein-Schumm Rule", the coupling between precipitation and erosion is still common. For example, a study across the Washington Cascades found a strong coupling between precipitation and long-term erosion rates (Reiners et al., 2003). A simulation model also predicts that erosion increases with increasing precipitation amount and precipitation intensity (Nearing et al., 2005). However, these discussions on the relationship between precipitation and erosion are often disconnected with the larger sociopolitical context.

Literature on the inquiry into the changing landscape in post-revolutionary China has bloomed in the last two decades. The analysis on correlations between land-use policy, land cover, and socio-economical vulnerability is a well-established one (e.g., Murphey, 1983; Xu et al., 2005). Driven by the desire to understand the effects of human intervention, many studies have analyzed the relationship between land cover and erosion characteristics and sediment yield in the upper Yangtze River (e.g. Zhang and Wen, 2004; Yin et al., 2011). However, few studies have tied together the discourses of policy, land use, and erosion at a fine spatial scale. More recent studies have combined geoscience and social science methods to unravel complex human landscape interactions and looked at linkages between governmental policies, headwater land

use, erosion, and downstream sedimentation (Collins et al., 2011; Urgenson et al., 2014). In this paper, I use similar approaches to synthesize the political ecology and geomorphic cause and effects of land use changes in rural Yunnan using a wide variety of data. It focuses primarily on post-revolutionary policies that directly or indirectly affected land use practices since the 1950s, as well as the effects of climatic and non-climatic factors on sediment yield.

Site Description

The basin of interest is less than 200 km^2 in size. Schmidt et al. (2011) indicated that large basins (>3000 km^2) have a stronger buffer capacity against extreme events, which can mask the change in sediment yield and erosion rates. This inverse relationship between sediment yield and drainage basin size has also been previously reported in the literature (e.g. Walling and Webb, 1996). As a result, this project will focus on a single small headwater drainage basin in Yunnan Province in order to tease out the relationship between land use and sediment yield.

The headwater drainage basin studied in this project lies within Weixi Lisu Autonomous County (hereafter Weixi County), one of the three counties that comprise Diqing (Dêqên) Tibetan Autonomous Prefecture in northwestern Yunnan (figure 1). The prefecture has experienced an average of 1.54% annual population growth since 1984 to 1991, similar to the province average of 1.57% (Yunnan Statistical Yearbook, 1984 and 1991). Weixi County stretches between 26˚53’ and 28˚02’ N, and 98˚54’ and 99˚34’ E. It has a total area of 4,661 km^2 and a population of 160,605 people, according to the 2010 census (Weixi County, 2012). Weixi County is also the hinterland of the UN World Natural Heritage “Three Parallel Rivers” area (figure 2). The Mekong River drains directly through the county, and the Salween and the Yangtze hug the county from its east and west. Although Weixi County is surrounded by UN

World Heritage protected nature reserve, it is not designated as protected nature reserve or scenic area (figure 2).

The Yong Chun River is the largest tributary of the main stem Mekong in Weixi County. It starts in the southeastern corner of Weixi County and flows northeastward until it drains into the Mekong River in Bajixun. Yong Chun River has a total length of 56km and drainage area of 811 km^2 (weixi.gov.cn). This project only looks at the headwater reach of Yong Chun River (figures 3 and 4), upstream of a hydrological gauging station that was built in the early 1960s. The total upstream area of this headwater basin (hereafter Weixi basin) is roughly 200 km^2. Although the study area has a relatively small drainage basin size, it has robust daily discharge and sediment concentration data from the early 1960s to the late 1980s.

Yunnan province is an interesting case as it has one of the highest poverty rates in China (Frayer et al., 2013) and hosts a large variety of ethnic minority groups whose religious beliefs have historically led to diverse land management strategies prior to collectivization by the government in the 1950s. Political change throughout the 20^{th} century has made it difficult to maintain consistent forest systems management (Menzies, 1994). Interestingly, Weixi basin lies in a region that has experienced extreme climate change over the last 25 years (Haynes, 2010), thus making it challenging to delineate anthropogenic effects on sediment yield independent of climatic factors.

Chapter Overview

This project is looking at the dynamic interphase connecting post-revolutionary politics, modern land use practices, precipitation patterns, and sediment yield records in Weixi basin. The ultimate goal is to identify what processes, climatic or not, account for the changes in local sediment yield and erosion budget. The project synthesizes information collected from various

sources, including remote sensed images, sediment and discharge records, precipitation records, and literature on land use policy changes (figure 5). These data cover slightly different periods of time but generally overlap between 1960 and 1987, thus providing a window of 27 years to tackle the linkages between sediment yield and its contributing factors.

The transport of suspended sediment in a drainage basin is a complex process responding to many variables including basin size, slope, precipitation, soils, runoff, and land use (Pizarro et al., 2014). This paper tackles the complicated question by first breaking into two smaller questions and then tying them back together. Chapter 2 explores in detail trends of precipitation, discharge, sediment concentration, and the correlation within. Chapter 3 describes the changing landscape of Weixi basin using remote sensing and short-lived radionuclide analyses. It also speculates about the correlation between upstream land use types and sediment erosional characteristics. Chapter 4 ties the previous analyses together by correlating the historical land use policies, quantified land use and land cover changes, precipitation patterns, basin average slope, and sediment yield in relatively fine spatial resolution. The combination of multiple analyses strives to elucidate how the watershed has responded to changes in precipitation or upstream land use land cover between 1960 and 1987.

Chapter 2. Sediment Yield and Climatic Influences

Introduction

In response to the blame on the central government's policy on land management for the exacerbated erosion in mountainous areas and ecological degradation in river valleys, I try to analyze if there is any long-term upward shifts in sediment yield in Weixi basin in this chapter. I start by analyzing interannual as well as seasonal trends of sediment yield. Sediment yield is often used as a proxy for understanding basin erosion because of its relative easiness in terms of measurements. However, a key distinction between the two concepts is that not all soils eroded will end up at the outlet of a basin, meaning that using sediment yield as a proxy will always underestimate the magnitude of erosion in the basin.

I also focus on precipitation, a key climatic factor that is thought to contribute to erosion in mountainous areas (e.g. Reiners et al., 2003). In order to characterize how precipitation affect the amount of suspended sediment transported in streams, I will examine separately the interannual variations in sediment yield and precipitation between the 1960s and the 1980s. Data used to analyze sediment yield include the amount and timing of the transport of suspended sediment in the channel.

Methods

I conducted a series of analyses to look at the interannual trend in discharge and sediment loading. The Ministry of Hydrology of the People's Republic of China measures daily discharge (m^3/s) and daily sediment concentration (kg/m^3) of Weixi Basin since 1960. The Ministry of Water Conservancy and Electric Power (1975) reported that data were collected using a Jakowski sampler and the standard 0.2-0.8 method. Data between 1960 and 1987 are available in

the form of published hydrology data books (Ministry of Hydrology, 1960–1987). The record of daily discharge measurements started on April 1, 1960 and the record of sediment concentration measurements started on June 1, 1963. Data are continuous between 1960 and 1987 except for the year of 1986, for which the book is missing. Calculations in this chapter only take into account years with a complete record. As a result, there are a total of 26 years of discharge data and 23 years of sediment data.

The analysis of temporal variations in sediment yield is threefold; all are calculated using numbers found in the published data books. I first calculated annual sediment yield for each year to identify any major temporal trends. I did so by multiplying daily discharge and sediment concentration, dividing by total watershed area and aggregating over one year.

$$Qs = \sum_{i=1}^{365} (TSS_i \times Q_i) \div A \tag{5}$$

Qs: sediment yield (kg/km^2/s)

TSS: total suspended sediment (sediment concentration) (kg/m^3)

Q: discharge (m^3/s)

A: basin area (km^2)

Because there is a large amount of data and the data were manually digitized, I performed a preliminary quality control screening by comparing annual sediment yield calculated from both mean annual value reported in the book summary and daily value from the complete dataset. I first calculated annual sediment loading from the reported mean annual sediment concentration and mean annual discharge (see equation 6); I also did the calculation based on the aggregation of daily sediment yield (see equation 5). The two values are within ±2% for all years.

$$Qs = \overline{TSS} \times \overline{Q} \div A \tag{6}$$

In addition to the interannual time series, I also analyzed cumulative daily sediment data by calculating the sum of total sediment yield since the April 1, 1960, the first day with reported sediment concentration. This approach of cumulative analysis has been previously used in detecting and quantifying the scope and amount of climate change anomalies (Lozowski et al., 1989, Haynes et al, 2010). It is applicable to analyzing sediment yield in this project because it eliminates the noise of random fluctuations within a year but captures consistent trends over time. The second derivative of the curve provides an estimate of the rate of change in sediment yield. The combination of time series of annual data and cumulative daily data will aid in capturing the signal in the trend of sediment yield in the basin.

Lastly, I plotted sediment rating curves for each year with sediment concentration on the y-axis and discharge on the x-axis in log-log space. Disturbance in a watershed is reflected in the upward shift in the slope or intercept of the regression of sediment rating curve as a result of increased sediment supply to stream channels (Environmental Protection Agency, 2012). For each year, I calculated the best fit line and looked for systematic changes in the parameters of the sediment rating curve.

Precipitation is a key factor in determining landscape morphology but is particularly hard to monitor in the mountainous area. High mountains are both difficult to access and encompass complex orographic effects. Both complexities call for a gridded precipitation dataset that monitors and interpolates rainfall with good spatiotemporal coverage. Existing historic, daily precipitation datasets for Asia include APHRODITE, TRMM-3B42(43), CPC-RFE, and GSMaP (Andermann et al., 2011). They come in different spatial and temporal resolutions and are derived from remote sensing observations and/or rain gauge data. Recent study has found that the APHRODITE_MA_V1003RI (Asian Precipitation Highly Resolved Observational Data

Integration Towards Evaluation of Water Resources, Monsoon Asia, Version 10) dataset provides the best temporal coverage in the Himalayas, and even estimates about daily precipitation are relatively accurate (Andermann, 2011). Although the test focuses on the Himalaya orogenic belt as its study area, my site location is in relatively close proximity and hence the adoption of the APHRODITE dataset should be a sound decision. APHRODITE is a distance weighted interpolated dataset from precipitation gauge stations and daily data are available between 1951 and 2007 (Yatagai et al., 2012). The amount of rainfall received in Weixi basin discussed later in the chapter comes directly from the APHRODITE dataset.

However, APHRODITE does not readily distinguish between snowfall and precipitation in early springs. I used a combination of MODIS/Terra monthly snow coverage data and Tropical Rainfall Measuring Mission (TRMM) satellite data to determine whether peaks in precipitation are actually due to rainfalls. MODIS/Terra is a gridded monthly dataset that records the percent land covered in snow since 2000 (Hall et al., 2006). I averaged monthly snow cover from 2000 and 2013 in order to get a representative snow cover for each month. Modern snow cover data are used as proxy for the amount of snowmelt during the period of interest in the project. A net decrease in snow cover suggests an influx of snowmelt into the river. TRMM_PR is a gridded precipitation dataset based on information collected from a meteorology satellite (Andermann et al., 2011; Anders et al., 2006). It captures diurnal and seasonal precipitation patterns but underestimates the total amount of rainfall by 15 to 25% because of the orbit of the satellite (Anders et al., 2006). I calculated the monthly averages of precipitation between 2000 and 2007 to get a representative seasonal trend in precipitation. Because the size of Weixi basin is smaller than the resolution of APHRODITE and TRMM, both of which are ~30* 30km, the precipitation data used in this project are directly from one pixel in these gridded datasets.

MODIS/Terra has a much finer resolution (~5*5km), and therefore a spatially weighted average was calculated. The adoption of multiple precipitation and snow cover datasets allows for a more confident interpretation of the precipitation patterns.

I analyzed the precipitation data using similar methods as I did for the sediment yield data. I first looked for temporal variations in precipitation by calculating cumulative daily precipitation to eliminate noise while keeping the signal (Lozowki et al., 1989, Haynes et al, 2010). I then compared the time series of precipitation with the time series of sediment yield to identify any co-variations in the general pattern. Although precipitation data is available since 1951, I only looked at dates that overlap with sediment and discharge data to make any comparison meaningful. I also plotted precipitation against discharge as obtained from the gauging station to explore the relationship between rainfall and runoff. The purpose of this analysis is to look for first-order responses of discharge to precipitation; therefore precipitation-discharge hysteresis is beyond the scope of this project. Finally, in order to analyze how precipitation, discharge, and sediment yield change seasonally, I took daily averages over the 26 and 23 years, depending on the variables, to produce a characteristic seasonal variation figure.

Results and Discussion

Sediment Yield

Annual sediment yield in Weixi Basin varies greatly between 1964 and 1987 (figure 6) with an average equal to 308 ton/km^2 and standard deviation of 469 ton/km^2. The two biggest exceptions occurred in 1979 (2023 ton/km^2) and 1984 (1377 ton/km^2), both of which are more than two standard deviation away from the mean. After removing the two outliers in the time

series, Weixi Basin has an average annual sediment yield of 175 ton/km^2 and standard deviation of 137 ton/km^2.

At a finer resolution, time series of daily sediment loading does not provide conclusive observations (figure 7a). The scattering of data points precludes the visual deduction of decadal trends. However, a plot of cumulative daily sediment loading displays a step pattern with relatively low angle slope for most months and an abrupt increase in slope for three to five months during a particular year (usually between May and October) (figure 7b). The two most prominent jumps in the cumulative sediment loading graph occur in 1979 and 1984, which is consistent with the annual sediment data. The step pattern is likely due to the fact that sediment mobilization occurs mostly during the monsoon season. Henck et al. (2010) found that sediment transport in the same region is dominated by monsoon flow rather than individual storm events. They concluded that mean monsoon flow is the effective discharge that mobilizes 86% of the suspended sediment.

The sediment rating curve of 23 years of data shows a moderate correlation between discharge and sediment concentration ($R^2 = 0.21$) (figure 8). A general hysteresis effect is observed in this figure. The loop shown in the graph might be seasonal differences in the amount of sediment available to be transported in the channel. A time series of slope and intercept of yearly rating curves displays a strong inverse correlation between slope and intercept of the best-fit line in log-log space for each year (figure 9). The average slope for the regression is 1.1 (STD=0.6) and the average intercept is 0.03 (STD=0.02). The changes in slope and intercept are possibly due to the hysteresis described earlier. A range of possible best fit lines exist, varying each year as the hysteresis changes its shape. The inverse correlation between the two parameters held constant through the record except for 1979 when both the slope and intercept went up

compared to the year before and the year after. The slope for 1979 is 1.25 ($p=0.27$) and the intercept is 0.09 ($p<0.001$). 1984 is another year of extremely high sediment loading. The regression between sediment concentration and discharge has a slope of 1.43 ($p<0.01$) and intercept of 0.01 ($p<0.001$). This shows that the same relationship between discharge and sediment loading was altered, suggesting that some other exogenous factors contributed to the peak in sediment loading that year.

When looking at the graph of daily sediment yield averaged over 23 years, there seems to be two clustered peaks of sediment loading event during the year (figure 10). The first one is a medium peak in late spring between March and April, and the other one is a larger peak that occurs between June and October. This graph provides information on the timing and mechanisms of sediment yield in the basin. The strong seasonality in sediment yield suggests that it might correspond to some climatic factors that also have strong seasonality, such as precipitation.

Precipitation

The comparison among the two precipitation datasets and the snow cover dataset proves to be very important in interpreting APHRODITE data. The monthly precipitation using APHRODITE shows a bimodal distribution of precipitation (figure 11-a). There is a peak in rainfall in March and April almost half the size of peak monsoon rainfall, which occurs between June and October. On the other hand, TRMM shows a clear monsoon precipitation signal (figure 11-b). MODIS/Terra data also shows that the percent land covered in snow drastically decreases starting in February (figure 11-c). By the end of April, almost all the snow has melted in Weixi basin. The combination of TRMM and MODIS/Terra data suggests that the peak of precipitation in APHRODITE is a false signal for precipitation, but rather a signal for snowmelt.

Although interannual variation exists (figure 12), the cumulative precipitation data shows a linear relationship with a steady slope and R^2 value of almost 1.00. This indicates that there is no trend for either increase or decrease in the amount of rainfall for the basin since early 1960. Although there is no long term change in precipitation during the window of analysis, sediment load does seem to respond to the increase and decrease in rainfall (figure 13). Except for the two years of peak sediment loading, there is a general trend of higher sediment load corresponding to higher precipitation. When taking 1979 and 1984 out of the equation, the R^2 value for the correlation between rainfall and sediment load increases from 0.07 to 0.54 (figure 14). This means that over half of the variance in sediment yield can be explained by the variance in precipitation, which is a relatively high correlation.

A close look at the relationship between precipitation, discharge, and sediment load in both 1979 and 1984 provides more information on what might have happened during those years (figures 15 and 16). Discharge responds strongly to precipitation events in the summer monsoon and snowmelt events in the spring. In 1979, there are two major peaks in sediment yield, one of which is in mid-June and the other one is in mid-October (figure 15). The latter corresponds to the peak monsoon rainfall; however, the former has similar magnitude of sediment yield as the one in October but does not follow a precipitation event half the magnitude of peak monsoon rainfall. This hyper response of sediment yield to precipitation could be due to a variety of reasons. The first one being some previous tectonic or climatic events had weakened the soil in the basin, making it more prone to erosion once the heavy rainfalls start in the summer. Another possible explanation is error in data entry in the hydrology book. In 1984, most sediment loading occurred during the monsoon season after intense precipitation events (figure 16). Again, the magnitude of sediment yield does not correspond to the average intensity of monsoon

precipitation. There is also another major sediment loading event in mid-April, likely triggered by the snow melting in Weixi basin.

In summary, although there is no long-term trend in precipitation for Weixi basin, precipitation is moderately correlated with sediment yield when looking at interannual variations. Precipitation also seems to affect seasonal fluctuations in sediment yield. Major sediment loading events correspond to spring snowmelt and monsoon rainfall. However, nothing in the precipitation record provides an explanation for why there are two years with anomalously large sediment yield. In the following chapter, I will explore other variables such as upstream land use and average slope that might provide more insight on this problem.

Chapter 3. The Changing Landscape

Introduction

This chapter explores a non-climatic factor in the larger story of basin erosion and sediment yield and seeks to explain the unusual peaks in the sediment yield record in 1979 and 1984. It strives to tease out the complex relationships between deforestation and erosion by first looking at the changing landscape between 1964 and 1990. It quantitatively assesses changes in land use and land cover (LULC) in Weixi Basin. The quantification of changes in LULC will provide more contexts for understanding how the local community responded to changes in governmental policy in their agricultural and logging practices.

In order to understand how LULC translate into erosion, I seek to connect land use history with modern erosional indices derived from short-lived radionuclide analyses. This chapter links the movement of sediments with upstream land use within Weixi basin with the hope to understand the source and mechanism of erosion. A combination of remote sensing and radionuclide analysis was used to elucidate the connection between upstream land use practices and erosional characteristics of the watershed.

Methods

Watershed boundary

Weixi basin is defined as the total area upstream of the local hydrology station. The Ministry of Hydrology (1960 – 1987) documents the location of the hydrology station (outlet) to the nearest minute and I ground-truthed the actual locality by correcting it to the logged GPS points taken at the station during summer 2013 fieldwork. I used ArcGIS to draw a watershed boundary for areas upstream of the hydrology station based on local topography. I first

downloaded a Digital Elevation Model (DEM) from the EarthExplorer (USGS). A DEM is a pixelated image with embedded elevation data and has a resolution of 30m. In order to ensure that rivers flow the correct direction in the basis, I burned previously digitized rivers into the DEM by making the cells that overlap with the streams 200m lower than they actually are. I used "fill" to eliminate any irregular holes that preexisted in the downloaded image, "flow direction" to calculate which direction water flows on the surface based on relief in the immediate surrounding area, and finally "flow accumulation" to delineate where water might accumulate as a result of the confluence of flow direction. I then adjusted the location of the station so that it is situated right on the nearest river where flow accumulates. I extracted a watershed boundary by using an operation called "watershed", which draws a boundary that encloses all the cells that contribute flows to the stream. I also calculated the total watershed area. The reported upstream area is 202 km^2 (Ministry of Hydrology, 1960–1987) and the calculated upstream area is 198 km^2 (< 2% error).

In order to think of the changing landscape of Weixi basin quantitatively and be able to assess the variation in land cover and erosion within this small basin, I divided the watershed into 15 small sub-watersheds based on the location of the samples collected in summer 2013. The precise location of sample collection was chosen for end-members in land use and slope before the field season. I repeated the steps described earlier to get boundaries of sub-watersheds. Weixi basin is composed of 15 sub-watersheds, the largest of which is 65 km^2 and the smallest is less than 1 km^2. Slope is calculated for each pixel within the DEM. Sub-watershed average slopes are calculated via "Zonal Statistics", which takes all the slope values within a sub-watershed and calculates basic statistics such as minimum, maximum, mean and standard deviation. This project only takes into account the mean slope for each sub-watershed.

Remote sensing

A previous study in the same region (Schmidt et al., 2011) found that there is a lack of correlation between sediment yield and land-use. The authors suggested that the inconclusive result could potentially reflect inaccuracies in the satellite images used in USGS classification. The land-use characterization in the previous study was done using Advanced Very High Resolution Radiometer (AVHRR), a radiation detection imager with a spatial resolution of 1km and temporal range from only 1992 and 1993. In this project, multi-temporal remotely sensed scenes taken at an interval of seven to ten years were downloaded from USGS Earth Explorer (Table 1).

Table 1. Imageries

Year	Date	Satellite	Resolution	# of Bands	Bands Used
1964	December 21	Keyhole-4A	2.74 meter	1	1; black and white
1974	January 5	Landsat MSS	60 meter	4	7,5,4
1981	October 19	Landsat MSS	60 meter	4	7,5,4
1990	November 4	Landsat TM	30 meter	7	4,3,2

I chose specific scenes based on the quality of the images (i.e. cloud cover), time of the year when images are available, and relative interval between two scenes. Images were captured by sensors installed on three different satellites: the CORONA KH-4A declassified spy satellites (USGS), Landsat Multi-Spectral Scanner (MSS) (USGS) and Landsat Thematic Mapper (TM) (USGS). The KH-4A image has high resolution (2.74 meter) and minimal cloud cover. It does not, however, support multi-spectral analysis as the film is panchromatic. Since the KH-4A image was not georeferenced, I used ArcGIS to define the geographical location of the image and clip out the basin of interest. This step increased errors in comparing this image to others because of some disproportional stretching during the process.

Two MSS imageries and one TM image were taken in 1974, 1989 and 1990. They were Level-1 product processed with the Standard Terrain Correction (USGS) and have projected coordinate system of Universal Transverse Mercator (UTM) with a WGS84 datum. Sensors on MSS and TM measure the intensity of light from multiple wavelengths ranging from 0.5 to 1.1 μm and 0.45 to 2.35 μm respectively (Table 2).

Table 2. Band characteristics for MSS and TM

Sensor	Band No.	Wavelength Interval **(μm)**	Spectral Response	Resolution (m)
MSS	4	0.5 - 0.6	Green	60
MSS	5	0.6 - 0.7	Red	60
MSS	6	0.7 - 0.8	Photo-IR	60
MSS	7	0.8 - 1.1	Near-IR	60
TM	1	0.45 - 0.52	Blue-Green	30
TM	2	0.52 - 0.60	Green	30
TM	3	0.63 - 0.69	Red	30
TM	4	0.76 - 0.90	Near IR	30
TM	5	1.55 - 1.75	Mid-IR	30
TM	6	10.40 - 12.50	Thermal IR	120
TM	7	2.08 - 2.35	Mid-IR	30

For the purpose of analyzing percent bare land in this project, I only used three bands to create a false color image (figure 17) and conducted further analyses for each time-period just on this image. I used ArcGIS operation "Band Composite" to create a raster dataset that has a specific band combination of R = NIR, G = Red, B = Green. The green band records green light reflected by chlorophyll and can be used to detect reflectance from healthy vegetation; the red band detects chlorophyll absorption in vegetation; near infra-red band records NIR reflectance peaks and is ideal for detecting water-land interfaces (Nelson and Geoghagen, 2002). When assigned with this band combination, the false color image shows vegetation cover in bright red and bare soil has a tan color. Water bodies appear blue; however, sediment-choked streams show

up as a lighter whitish blue and can be hard to distinguish from urban areas, which are typically blue-gray in color (Nelson and Geoghagen, 2002).

The quantification of land cover change is complicated as the four images come in different resolution, format, and band composition. In order to calculate the change in % bare land between 1964 and 1990, I used "Iso Cluster Unsupervised Classification". This tool assesses the signals from one or multiple input bands for each pixel and groups clusters of pixels into one classification based on similarity. The number of classes varies between four and seven for all four images in order to minimize the effect of intense shadow in mountainous area and get the best representative signature. I then used an Arc tool "reclassify" to reassign classification for each pixel; initial classes that represent the same type of land cover are grouped into one. The reclassified image has only two distinct groups: forest and bare land. The alternative method of quantifying land cover change is drawing freehand to trace the contour between forest and cleared land, which could introduce more error from manual tracing and is thus not adopted. After I classified each individual pixel of the image, I converted the raster file into a shapefile using "Raster to Polygon", which preserves only the boundary information between two different classes. I also overlaid the land cover file with the delineated watershed boundary to calculate percent bare land in each sub-watershed.

Short-lived Radionuclide

^{137}Cs is an anthropogenic product of nuclear weapon testing since the 1950s and has a half-life of 30.17 years. After ^{137}Cs fallout is deposited in soil and sediments, it stays with the particles because of the strong adsorption to clay minerals (Porêba, 2006). ^{210}Pb is a natural product of the uranium decay series, with a half-life of 22.26 years. It is derived from the decay of ^{222}Rn, which in itself is the daughter of ^{226}Ra. The isotope ^{226}Ra occurs naturally in rocks and

soils and is constantly decaying into ^{210}Pb; the two isotopes are in equilibrium with each other. However, since ^{222}Rn occurs in gaseous form and may escape from the sediment, a small fraction of the isotope introduces ^{210}Pb into the atmosphere. When ^{210}Pb settles in the topsoil and sediments as atmospheric fallout, it is no longer in equilibrium with its parent ^{226}Ra and is called "unsupported ^{210}Pb".

The method of using fallout radionuclides concentration as a fingerprint allows us to infer the source of suspended river sediments (Walling and Woodward, 1992). Both unsupported ^{210}Pb and ^{137}Cs are used to fingerprint sediment sourcing because different amounts of radionuclide are associated with different depth and characteristics of soil (figure 18). Walling and Woodward (1992) suggested that sediments sourced from undisturbed soil will have a higher concentration than those from cultivated soil because ploughing and cultivating disturb the accumulation in the surficial layer. Similarly, deep erosion that penetrates below the upper horizon as well as rapid erosion that precludes accumulation will both lead to low concentrations of fallout radionuclide. Using more than one nuclide with different fallout histories and decay rate also helps to pinpoint the source and mechanism of erosion (Walling and Woodward, 1992). If a sample of sediments has high activity in both unsupported ^{210}Pb and ^{137}Cs, it was most likely transported during shallow, slow erosion. An absence or very low activity in both nuclides suggests either long-term high rates of erosion or deep erosion.

Fifteen river sediment samples were collected from in-channel river bottoms in summer 2013 in Weixi Basin at various segments and junctions of streams (figure 19, table 3). Sediments were sieved into 250-850μm fractions at site, oven-dried and packed into plastic containers in the lab. I used a Canberra gamma counter broad energy germanium detector (BE3830) with a vertical dipstick cryostat to measure abundance of short-lived isotopes. Most samples were

counted for 24 hours for unsupported ^{210}Pb or ^{137}Cs. A few samples were run for 48 hours to see how it affected counting statistics. The doubling in counting time improves counting statistics by lowering uncertainty in the peak energy by a factor of 1.4 because errors scale with the square root of the number of counts.

Table 3. Sub-watersheds with unsupported ^{210}Pb and ^{137}Cs

	Sample location		Counting time (s)	Unsupported ^{210}Pb		^{137}Cs	
Sub-watershed	Lat.	Lon.		Activity (bq/g)	Error %	Activity (bq/g)	Error %
1	27.16	99.32	86400	7.208	35.7		
3	27.15	99.41	86400				
4	27.13	99.41	172800				
5	27.13	99.41	86400				
9	27.13	99.41	86400	4.378	59.0		
10	27.12	99.35	172800				
11	27.12	99.36	86400	6.112	51.0		
12	27.12	99.35	86400				
13	27.08	99.35	86400	8.748	25.7	0.023	81.8
16	27.07	99.35	86400			0.028	68.7
17	27.07	99.35	86400	4.883	46.2		
20	27.06	99.35	86400				
21	27.06	99.36	86400	4.344	63.7		
23	27.06	99.35	86400	5.350	48.6		
24	27.06	99.36	86400	5.577	46.5		

To measure the amount of each radionuclide within each sample, an empty container is counted twice first, each time for 48 hours to calculate background gamma decay that is occurring in the container itself or in the measuring space. The background count was scaled to 24 hours and then subtracted from all measurements before any further calculation. The spectrum analysis software was preset to count within defined channels, each corresponding to specific peak energies of certain radionuclides (table 4).

Table 4. Energy peaks of interest

Nuclide	Energy (KeV)	gamma decay fraction
^{210}Pb	49.5	4.05%
^{214}Pb	295.2	19.2%
^{214}Pb	351.9	37.1%
^{214}Bi	609.3	46.1%
^{137}Cs	661.7	85%
^{214}Bi	1120.3	15%
^{214}Bi	1764.5	15.4%

Unsupported ^{210}Pb is calculated by subtracting the average of four proxies for supported ^{210}Pb (^{214}Pb at 295.2 keV and 351.9 keV, ^{214}Bi at 609.3 keV and 1120.3 keV) from the total ^{210}Pb (49.5 KeV) measured directly through gamma decay. Although ^{214}Bi at 1764.5 KeV is another proxy for supported ^{210}Pb, it is excluded from the calculation as its activity is unexpectedly higher than the other four proxies for all samples (figure 20).

The specific activity (A_s) measures the radioactivity within the samples and is a function of number of counts (N), counting efficiency (ε), counting time (t), mass (m), percent of gamma decay (P_γ), half-life ($t_{1/2}$), and time since samples collected (t_o).

The Germanium detector reports concentration of nuclides in counts (N). I also used ANGLE, a semiconductor detector gamma-efficiency calculations software to calculate efficiency (ε) based on geochemical composition of samples as well as the geometric shape and composition of the container (Mihaljević et al., 2012).

$$N = A \times t \times \varepsilon \quad (1)$$

The total activity was then normalized by mass and fraction of decays which are gamma decays (P_γ).

$$A_{total} = A \div P_\gamma \div m \quad (2)$$

Lastly I corrected the specific activity (A_s) for the amount of radioactive decay since t_o in order to make different samples comparable. t_o was defined as sample collection date for

unsupported ^{210}Pb. However, activities for ^{137}Cs were normalized to a date prior to any collected samples because there was no more ^{137}Cs fallout occurring any more.

$$\frac{A_{t_o}}{A_{total}} = 2^{-\frac{t_o}{t_{1/2}}} \quad (3)$$

Specific activity is reported in the SI unit, Becquerel per gram (Bq/g) for all samples. Errors were calculated from the reported percent error from the initial count.

The combined equation is thus:

$$A_s = \frac{N}{\varepsilon \times t \times m \times P\gamma \times 2^{-\frac{t_o}{t_{1/2}}}} \quad (4)$$

Lastly, I performed a statistical significance test to compare the land use and land cover between sub-watersheds that have detectable amounts of unsupported ^{210}Pb or ^{137}Cs and sub-watersheds that do not.

Results and Discussion

Weixi basin has a total upstream area of 198.01 km^2, of which 77.2% is forested and 22.8%[1] is cleared for grazing, farming, urban area, and other purposes. The mean elevation is 2930 m and the mean slope is 19.1^o (table 5). Most bare land is located in valley bottoms, whereas mountain slopes remain mostly forested (figure 21). Total percent bare land increased between 1964 and 1974, but has since then decreased from 24.4% to 20.2% between 1974 and 1990 (figure 21, table 6). A total area of 8.3 km^2 was reforested during the 16 years.

Multi-temporal satellite images cover a total span of 26 years; however, extrapolating LULC information of the years in between based solely on the four classified instances is extremely problematic. Although there was less cleared land in 1990 than 1974, there could have still been more land clearing after 1974. Yet such change would not have been captured by the

[1] This is calculated by averaging the four years (1964, 1974, 1981, and 1990).

coarse temporal resolution used in this project. It is also important to know that the land cover map was calculated from images of very different resolution. Patches of mixed land cover might not be distinguishable in coarse resolution images. Similarly, because rivers appear to be dark gray in the panchromatic image of 1964, "Iso Cluster Unsupervised Classification" was unable to distinguish rivers from dark canopy (figure 22). On the contrary, it successfully classified streams in the "non-forested" land cover type for all of the other three multi-spectral images. However, I did not correct the classification because the number of total pixels misclassified as forest cover in the 1964 image is much smaller than the size of the average sub-watershed. Because of the inconsistent resolution from all four images, the confidence level of the temporal changes in land use and land cover is not very high. But even with a rough preliminary classification, the percent bare land ranges between 20% and 25% for four years, suggesting that the methods used are somewhat robust.

Table 5. Sub-watershed characteristics in 1990

Basin	**Area (km^2)**	**Average Slope**	**Average Elevation (m)**
1	66.34	21.03	2894.3
3	5.24	17.97	3163.8
4	5.79	21.60	2978.0
5	4.91	15.86	2751.7
9	1.88	17.37	2677.6
10	6.44	21.94	3049.3
11	7.73	22.40	2974.4
12	2.25	21.08	2729.2
13	13.56	10.81	3297.3
16	4.96	19.55	3181.0
17	17.66	16.13	3195.1
20	0.13	28.88	2730.4
21	28.42	18.79	2787.4
23	4.81	15.21	2559.2
24	27.90	20.11	2812.4
Total	**198.01**	**19.13**	**2930.9**

Since I was unable to confidently use temporal land use and land cover changes to correlate with the sediment yield record, I used "space-time substitution" to explore the effect land use has over erosion and sediment yield. The spatial heterogeneity in Weixi basin is utilized to compare LULC and erosion characteristics among sub-watersheds. The 15 sub-watersheds have different characteristics including mean elevation, mean slope, and percent of cleared land (table 5and 6). Most headwater watersheds have lower percent of cleared land compared to middle-lower basin except for the southernmost sub-watershed (figure 23).

Table 6. Land cover in sub-watersheds in 1964, 1974, 1981, and 1990

	1964	**1974**	**1981**	**1990**	**average**
Sub-Watershed	% cleared land	% cleared land	% cleared land	% cleared land	% cleared land
1	22.5	30.7	30.6	23.0	26.7
3	16.1	11.1	6.0	4.5	9.4
4	19.3	15.7	15.5	7.8	14.6
5	26.9	27.6	25.5	27.3	26.8
9	30.6	30.6	29.6	30.2	30.3
10	28.3	16.8	14.3	12.8	18.1
11	13.9	11.8	17.3	9.3	13.1
12	16.3	11.3	12.2	14.0	13.5
13	20.5	23.7	9.2	25.3	19.7
16	13.5	13.1	12.2	13.9	13.2
17	28.2	28.7	11.2	18.6	21.6
20	66.5(*)	34.2	16.0	17.4	22.5 (*)
21	22.3	18.1	20.6	16.1	19.3
23	31.5	34.4	36.1	33.7	34.0
24	28.6	23.2	29.8	23.9	26.4
Total	**23.4**	**24.4**	**23.0**	**20.2**	**22.8**

* Sub-watershed 20 is averaged for three years because of a georeferencing error in 1964.

Although Weixi basin experienced net reforestation since 1974, not all sub-watersheds followed the same trend as shown in figure 24. Sub-watersheds with a net increase in land clearing are shown in shades of red, whereas those with a net decrease in land clearing are shown

in shade of green. The analysis of changes in land cover at sub-watershed scale is divided into two periods, the first one being 1974 to 1981, and the second being 1981 to1990.

Four sub-watersheds in the lower-middle basin (basins 11, 21, 23, 24) showed a significant (>1%) increase in percent of cleared land between 1974 and 1981 even though the overall basin average decreased. Cleared land increased by 28.4% and 27.9% respectively in basins 21 and 24. Sub-watersheds close to the headwaters, on the other hand, showed significant decreases in cleared land, more consistent with the overall basin average. Basins 13 and 17 had the highest rate of reforestation of 14.5% and 17.5%. Basins 1, 4, 9, 12, and 16 had no significant change in land cover in the first period. During the second period between 1981 and 1990, an almost opposite phenomenon can be observed. Three headwater basins in the southernmost basin and the northeastern basin showed varying degrees of deforestation. Basins 13 and 17 experienced a 16.0% and 7.4% increase in % land cleared. The previously reforested sub-watersheds showed signs of deforestation, whereas previously deforested lower sub-watersheds showed between 2.5% to 8% decrease in land clearing.

Zonal statistics on the relationship between slope and land cover change show similar results (table 7). During the first period (1974 – 1981), reforestation happened in low slope, high elevation area and deforestation happened in high slope, low elevation area. However, during the second period (1981-1990), reforestation happened in high slope, low elevation area and deforestation happened in low slope, high elevation area.

Although there seems to be an apparent switch of deforestation and reforestation pattern, we do not know whether the reversal in land cover changes occurred on the same patches of land. The apparent reversal between deforestation and reforestation pattern could also be a result of mixed spatial resolution and classification errors. For example, basin 13, 16, and 17 are all

pasture land. Because I only used two categories for LULC classification, pasture land sometimes gets classified as forested land whereas other times it get classified as cleared land based on the time of year and the wetness of the soil. The 1981 image was taken in October, which is earlier than the other three images. The fact that Weixi basin was still under the influence of monsoon rainfall means that the pasture could be wetter and greener, making it more likely to be classified as forested land.

Table 7. reforestation and deforestation pattern

	reforestation		**deforestation**	
	slope	elevation	slope	elevation
1974-1981	14.14	3053.40	22.36	2834.74
1981-1990	22.67	2860.17	13.97	2946.57

Short-lived radionuclide data also revealed some information about the erosional characteristics of the sub-watersheds in Weixi basin. Among the total 15 sub-watersheds, eight of them have detectable amounts of unsupported ^{210}Pb and two have detectable amount of ^{137}Cs in the samples collected (table 3, figure 25). I chose a cutoff error of 65% for reportable amount of ^{210}Pb and 85% for ^{137}Cs. Mabbit et al. (2008) suggested that low precision on the estimate of unsupported ^{210}Pb is common and the uncertainty can be as high as ±50% when concentration is low. I further increased the cutoff for both radionuclides because of the relatively short counting time and low concentrations in the samples.

The only two headwater sub-watersheds (basin 13 and 16) that show traces of ^{137}Cs are in the northeastern basins (figure 26). Most of Weixi basin has no ^{137}Cs present at all, suggesting that there had been massive erosion since the 1960s that eroded away all of the near-surface soils that contained any ^{137}Cs. Land cover for these two sub-watersheds is pasture (figure 26), which might explain the presence of ^{137}Cs. Sediments that have ^{137}Cs generally source from slower erosion. These two sub-watersheds might have been utilized in similar ways since early human

settlement and remained the same land use/land cover during the modern deforestation periods. Relatively lower frequency of disturbance compared to the rest of Weixi basin in the two sub-basins could explain signals of slower erosion.

Unsupported ^{210}Pb is present in most of the sub-watersheds. For sub-watersheds that have unsupported ^{210}Pb but no ^{137}Cs, this scenario could mean that there had been intensified erosion since the 1960s but had also since stabilized, allowing for ^{210}Pb accumulation in the soil profile. Not surprisingly, basin 13, which was one of the two basins that had ^{137}Cs, also had the highest activity for ^{210}Pb, suggesting a slow, and shallow erosion. However, the sub-watershed immediately downstream of basin 13 (basin 16) shows low ^{210}Pb activity. Similarly, sub-watershed 11 has high activity but the downstream basin 12 has very low activity. There are two possible explanations for this pattern. The high activity sediments found in upstream basin might be stored somewhere between the two sample sites, such as alluvial fans where there is a sharp change in slope. On the other hand, the upstream basin might only contribute small amounts of high activity sediments, and when they are mixed with other influx of sediments from the basin immediately downstream of the upstream one, the dilution of activity makes ^{210}Pb undetectable by the machine.

Table 8. T-test – correlation between the presence of unsupported Pb and Cs and land use

	Groups	Count	Sum	Average	Variance	P-value
Land use (% bare land)	unsupported ^{210}Pb	8	190.88	23.86%	45.33	0.055
	no ^{210}Pb	7	118.04	16.86%	36.43	
	^{137}Cs	2	32.837	16.41%	21.19	0.396
	no ^{137}Cs	13	276.09	21.23%	54.77	

The statistical significance test (α=0.1) compares the mean percent bare land between sub-watersheds that have detectable amounts of unsupported ^{210}Pb or ^{137}Cs and sub-watersheds that do not (table 8). There is no significant difference in percent bare land between sub-

watersheds with and without detectable amounts of ^{137}Cs. This could be because there are only two sub-watersheds with ^{137}Cs. Sub-watersheds with detectable amounts of unsupported ^{210}Pb have higher percentage of bare land; the ones with ^{210}Pb have an average of 23.8% cleared land, whereas the ones without unsupported ^{210}Pb have an average of 16.9% cleared land (P=0.055). This result is completely opposite of what one would have expected. Deforestation is thought to contribute to the decrease in soil cohesion and increase in erosion; hence the absence of ^{210}Pb is associated with fast and deep erosion. But in the case of Weixi basin the absence of ^{210}Pb happens in basins with less cleared land.

One possible explanation for the seemingly contradictory results is the existence of another confounding variable that is responsible for changes in both land use and depth of erosion. Slope is one possibility. It is likely that people in Weixi preferentially deforested areas with shallower slope because those lands are more stable and more suitable for farming. At the same time, shallower slopes are more stable and more likely to have shallow and slow erosion compared to steeper slopes. The statistical analysis that compares the basin average slope between sub-watersheds that have detectable amounts of unsupported ^{210}Pb or ^{137}Cs and sub-watersheds that do not confirms such hypothesis (table 9). The analysis shows a weak significance in slope for both ^{210}Pb and ^{137}Cs. Mean slope is less steep for sub-watersheds with either of the radionuclides, meaning that sediments found in watersheds with either radionuclide are sourced from shallower slopes.

Table 9. T-test – correlation between the presence of unsupported Pb and Cs and slope

	Groups	Count	Sum	Average	Variance	P-value
Slope (degree)	unsupported ^{210}Pb	8	141.84	17.73	13.78	0.131
	no ^{210}Pb	7	146.8	20.98	16.82	
	^{137}Cs	2	30.35	15.17	38.23	0.138
	no ^{137}Cs	13	258.3	19.87	13.37	

Chapter 4. The Story of Weixi Basin

Weixi basin has a total upstream area of 198 km^2 and averages 2930.9m in elevation and 19.13 degree in slope. As of 1990, the basin has 20.2% bare land. This project explores the previously unexplored relationship between sediment yield and other factors such as precipitation, land use/land cover of the basin. Data from various sources and overlapping time period allow us to piece together a cohesive narrative of the story of Weixi basin**.** The story also links the change in forest management policies and the change in sediment yield, which opens up a unique window to analyze quantitatively how post-revolutionary policies have shaped the landscape and sediment load in the basin.

Calculations of sediment yield reveal that the basin has a relatively stable amount of suspended sediment transported throughout the examined time period with the exception of 1979 (2023 ton/km^2) and 1984 (1377 ton/km^2). The average sediment loading is 175 ton/km^2 (STD=137) when those two years are treated as outliers. Most of the sediment is transported during the monsoon season when there is a period of concentrated intense rainfall events.

Precipitation did not systematically change during the period of examination despite previous speculation of change in rainfall pattern resulting from extreme climate change (chapter 1). The straight line with constant slope in cumulative precipitation figure shows that there is no increase or decrease in the amount of rainfall despite seasonal variations (figure 12b). However, when looking at the time series of mean annual precipitation together with sediment load, the two curves possess similar trends (figure 13). With the exception of 1979, sediment yield tends to increase when there is a year of heavier rainfall and vice versa. The fact that precipitation did not change over the long run does not necessarily mean that it does not have any effect on sediment yield. On a decadal temporal scale, the interannual oscillation observed in the time

series of sediment yield appears to be directly linked to precipitation. When excluding the two years with extreme sediment yield, the regression between sediment yield and precipitation became more linear; the R^2 value increased from 0.07 to 0.54 ($p<0.001$) (figure 14), suggesting that variance in rainfall explains over 50% of the variance in sediment yield data. On a seasonal scale, monsoon rainfall is the single biggest driving force that mobilizes sediments in the streams (figure 10). Yet the peaks in 1979 and 1984 cannot simply be explained by this climatic factor. In 1979, the spike of sediment yield corresponds to a decrease in precipitation, the exact opposite of the trend observed in previous years. Combined with the deviation of the two parameters of the sediment rating curve, some other factors must have contributed to the massive loading of suspended sediments in the stream channel. In 1984, although sediment yield and precipitation followed the same upward trend, the magnitude of response to precipitation is greater than any previous years, suggesting that the increase in sediment transported might not be explained by the increase in rainfall alone.

To sum up the effects of the climatic factor on sediment yield, interannual variability in precipitation accounts for most but not all of the fluctuations of sediment yield in Weixi basin. Reasons other than rainfall should be responsible for the spike of sediment loading in 1979 and 1984. The disconnect between precipitation and sediment yield in those two years could be due to changes in land use and land cover, or other tectonic or climatic events that weakened the soil, making it more prone to erosion once snowmelt or monsoon rainfall starts.

Another possible explanation of the anomalies is errors that occurred in data entry in the book published by the Ministry of Hydrology. The peak in sediment yield in response to a rainfall event in early July in 1979 is significantly higher than the rest of the year. It is possible that one particular data point is erroneous in that year. However, the calculated average of that

year is consistent with the reported mean sediment yield in the data book, suggesting some level of credibility in the data entry process.

Although changes in and use/land cover was hypothesized to contribute to the destabilization of watershed and the anomalous peaks in 1979 and 1984, I was unable to make strong conclusions on temporal changes in LULC. Data used to understand the history of land use in Weixi basin between 1964 and 1987 is not continuous, but still reveals some trend of clearing and reforesting in the basin. The increase in percent bare land between 1964 and 1974 is likely a result of a combination of the Great Leap Forward movement and the Cultural Revolution. In the 1950s through 1970s, forests were cut down for fuel as well as for clearing for agriculture. In the attempt to rapidly industrialize and catch up with the Western world, forests were cleared to stoke thousands of backyard steel furnaces during the Great Leap Forward. Even more land was cleared for cultivation of grains during the Cultural Revolution. The increase in percent bare land in Weixi basin between 1964 and 1974 almost certainly extended back to 1958 when the Great Leap Forward movement was launched.

The land use/land cover map of 1984 suggests that less land is cleared than in 1974. However, the decrease in percent bare land possibly did not occur until close to the 1980s since no systematic reforestation policy was implemented until early 1980s in Yunnan (Elvin and Liu, 1998). The change in land use/land cover between 1974 and 1984 can be summed up as a net deforestation at high-slope-low-elevation land and a net reforestation at low-slope-high-elevation land. The mean slope and elevation for additionally cleared land during that period is 22.3 degree and 2835 meters; the mean slope and elevation for replanted land is 14.1 degree and 3053 meters. On the contrary, the change between 1984 and 1990 shows a net deforestation at low-slope-high elevation land and a net reforestation at high-slope-low-elevation land. The mean

slope and elevation for deforestation and reforestation is respectively 14 degree, 2946 meter, and 22.7 degree, and 2860 meter. It suggests that people in the area had reforested what was previously deforested, yet cleared more land that was previously reforested. Although there is some error associated with land use/land cover classification because of the difference in spatial resolution of the images, the two distinct patterns of net reforestation seen in these two periods might be linked with the policy banning high slope agriculture (Elvin and Liu, 1998).

For further studies on changes in land use/land cover, a better quality control should be adopted to make images between four years more comparable. One suggestion is to create a standard for all four images. For example, one could resample the images so that they are all grayscale images with a resolution of 60m, and compare the classification results with the current ones. This might elucidate how multi-spectral analysis and fine resolution could skew the land use/land cover information.

The short-lived radionuclide analysis provides some useful information on interpreting the modern erosion characteristics of the watershed. It suggests that land use is not significant, or at least not in the direction that we have hypothesized, for depth of erosion in Weixi basin. Instead, the results show that shallow slopes correlate with slow erosion whereas steep slopes are correlated with faster or deeper erosion, suggesting that slope is a much bigger control on where river sediments are sourced in the watershed. This is consistent with the concept that hillslopes at higher angles are less stable and more likely to have landslides and other erosional features.

Errors for both ^{210}Pb and ^{137}Cs are extremely high, thus no affirmative conclusions should be drawn. However, samples have relatively low or none activity for ^{137}Cs, suggesting that a lot of erosion has occurred since the 1960s, eroding away all the surficial layers of soil that

contained fallout ^{137}Cs. For future studies of the same basin, samples that show detectable amounts of either ^{210}Pb or ^{137}Cs should be counted for longer to reduce the percent errors.

Although the detailed record of sediment yield between 1964 and 1987 allowed me to accomplish some analyses of Weixi basin, it unfortunately does not extend back to the first decade of the foundation of the country or forward through the more recent environmental protection policies. The first major deforestation period associated with the Great Leap Forward predates the beginning of any documentation on sediment concentration in the basin, making it impossible to make comparisons with pre-modern China. Similarly, the lack of information on more recent changes in sediment yield precludes any further analysis on how the basin responded to the economic reform and embrace of market based economy. To further link the change in land use/land cover with the trend we discuss earlier in sediment yield, the extremely high yield of suspended sediment in 1979 could be a result of massive clearance of land in the watershed the previous year. However, no specific policies can be directly linked temporally to either of the two large sediment loadings in 1979 and 1984. The abnormal response to rainfall in 1984 could suggest increasing vulnerability in the watershed; however, the lack of data past 1987 makes it impossible to assess any long-term trends beyond the available data. More current information on how the watershed is responding to the continuous disturbance would be necessary to conclude whether this mountainous area is becoming more prone to erosion.

Another drawback of this study is the lack of first handed information on the influence of national forest management policies on the local community. Most literature focuses on the national scale changes (e.g. Murphey, 1983) and few focus on the implementation of new policies in a province scale (e.g. Marks, 2012). But the effectiveness of forest management policies trickling from the state level to the municipal level in the mid-1900s is highly

questionable. The question of how local people responded to the shift in ownership and other forest-related policies will remain puzzling without doing field interviews.

This multidisciplinary project addresses many facets of the complicated story of a rapidly changing landscape in a rural mountainous watershed in post-revolutionary China. It reveals that the amount of suspended sediment transported in rivers is concurrently influenced by precipitation and land use changes. Although the intricacy in the balance between the two factors is still unclear at this point, this paper builds important causal linkages between the land use policy and the changes in the watershed in terms of geomorphic processes. Future studies could focus on other watersheds in different climate zones or of different sizes. More emphasis should be placed on conducting field interviews with local residents to improve the understanding of the effect of national policies on a local level.

Acknowledgements

I would like to thank my advisor, Amanda Schmidt for her invaluable help mentoring and supporting me throughout the duration of this process. I would also like to thank Karla Hubbard and Carlo DeMarchi for being on my committee and providing helpful feedback. I would also like to acknowledge the National Science Foundation for the supporting the project, Christoff Andermann for the APHRODITE and MODIS data, Adrian Singleton for digitizing rivers, Ari Goodman for remote sensing help, the field team (Amanda Schmidt, Thomas Neilson, Veronica Sosa Gonzalez, Jenny Bower, Wei Renjuan, Zhang Chunmin) for helping collecting all of my samples in summer 2013, and the lab crew (Adrian Singleton, Dom Fiallo, Gaby Garcia, Katie Dunn) for running the samples. I would also like thank my fellow honors students (Jack, Katie, Will, Katrina) for making this process fun and enjoyable!

Works Cited

Andermann, C., S. Bonnet, and R. Gloaguen. 2011. Evaluation of precipitation data sets along the Himalayan front. *Geochemistry Geophysics Geosystems* **12**(7):1-16.

Anders, A., G. H. Roe, B. Hallet, D. R. Montgomery, N. Finnegan, and J. Putkonen. 2006. Spatial patterns of precipitation and topography in the Himalaya. In *Tectonics, climate, and landscape evolution*, ed. S. D.Willett, N. Hovius, M. T. Brandon, and D. Fisher, 39–53. Boulder, CO: Geological Society of America.

Buckley, M. 2011. Three parallel rivers UN World heritage site. http://www.meltdownintibet.com/f_biodiversity.htm Last accessed: April 29, 2014.

Burbank, D.W., A. E. Blythe, J. Putkonen, B. Pratt-Sitaula, E. Gabet, M. Oskin, A. Barros, and T. P. Ojha. 2003. Decoupling of erosion and precipitation in the Himalayas. *Nature* **426**: 652-655.

Campbell, J. B., and R. H. Wynne. 2012. *Introduction to remote sensing*, fifth edition. 5. New York, NY: The Guilford Press. Print.

Chen, G. J. 2000. Major causes of soil erosion in the Upper Yangtze River valley and the control countermeasures (in Chinese). *Rural Eco2Environment* **16**(3), 5-8.

Collins, B. D., A. H. Schmidt, S. Harrell, 2011. Soil erosion, fluvial processes, and land use history in a mountainous catchment in southwest Sichuan Province, China. In *Association of American Geographers Annual Meeting*, Seattle, WA.

Environmental Protection Agency. 2012. Integration of stream stability, reference condition & sediment rating curves. In *Watershed assessment of river stability & sediment supply*. Washington, DC: Environmental Protection Agency. http://www.epa.gov/warsss/sedsource/rivrelat.htm (last accessed 25 March 2014).

Fearnside, P. M., and W. F. Laurance. 2004. Tropical deforestation and greenhouse-gas emissions. *Ecological Applications* **14**(4): 982–986.

Giri, Chandra. 2012. *Remote sensing of land-use and land cover*: Principles and Applications. Boca Raton: CRC Press. Print.

Hall, D. K., Salomonson, V. V., and Riggs, G. A. 2006. MODIS/Terra Snow Cover Monthly L3 Global 0.05Deg CMG, Version 5. Version 5.0., Boulder, Colorado, USA: National Snow and Ice Data Center.

Haynes, M. 2010. Rapid climate change in NW Yunnan (phD dissertation at Univeristy of Wisconsin-Madison).

Henck, A.C., D.R. Montgomery, K.W. Hunrington, and C. Liang. 2011. Monsoon control of effective discharge, Yunnan and Tibet. *Geology* **38**(11): 975-978.

Hooke, R. L. 2000. On the history of humans as geomorphic agents. *Geology* **28**(9), 843-846.

Hooke, R.L., J. F.Martín-Duque, and J. Pedraza. 2012. Land transformation by humans: aA review. *GSA Today* **22**(12): 4-10.

IPCC, 2000. *Land use, land-use change and forestry.* Watson R.T. I.R. Noble, B. Bolin, N.H. Ravindranath, D. J. Verardo, and D.J. Dokken, eds. UK: Cambridge.

Jha S., and K. S. Bawa. 2006. Population growth, human development, and deforestation in biodiversity hotspots. *Conservation Biology* **20**(3):906–912.

Langbein, W. B., and Schumm, S. A. 1958. Yield of sediment in relation to mean annual precipitation. *Am. Geophys. Union Trans* **39**, 1076-1084.

Long, H. L., G. K. Heilig, J. Wang, X. B. Li, M. Luo, X. Q. Wu, and M. Zhang. 2006. Land use and soil erosion in the upper reaches of the Yangtze River: some socio-economic considerations on China's Green-for-Green Program. *Land Degradation and Development* **17**(6): 589-603.

Lozowski, E. P., R. B. Charlton, C. D. Nguyen, and J. D. Wilson. 1989. The use of cumulative monthly mean temperature anomalies in the analysis of local interannual climate vaiability. *American Meteorological Society* **2**: 1059-1068.

Lu, X. X., and D. L. Higgitt. 1998. Recent changes of sediment yield in the Upper Yangtze, China. *Environmental Management* **22**:697–709.

Marks, R.B. 2012. *China: Its environment and history.* Rowman & Littlefield Publishers. Lanham, Md. Pp 285-287.

Menzies, N.K. 1994. *Forest and land management in Imperial China.* St. Martin's Press, London

Murphey, R. 1983. Deforestation in Modern China. In: P.T. Richard and J.F. Richard (eds.), *Global Deforestation and the Nineteenth Century World Economy.* Duke Press Policy Studies. New Haven, USA. Pp. 111-128.

Ministry of Hydrology. 1960–1987. Zangdian Guoji Heliu Shuiwen Ziliao (District 9 Region 2 1947–1987). Yunnansheng Shuiwen Zongzhan Geming Weiyuanhui Kanyin.

Ministry of Water Conservancy and Electric Power. 1975. Handbook for hydrological survey. Beijing: Water Conservancy and Electric Power Press.

Nearing, M. A., V. Jetten, C. Baffaut, O. Cerdan, A. Couturier, M. Hernandez, Y. Le Bissonnais, M. H. Nichols, J. P. Nunes, C. S. Renschler, V. Couchere, and K. van Oost. 2005. Modeling response of soil erosion and runoff to changes in precipitation and cover. *Catena* **61**:131-154.

Neilson, T. B. 2013. Determination impacts of land-use on erosion and sediment dynamics in southwestern Chinese rivers using cosmogenic ^{10}Be and short-lived radiogenic isotopes (Thesis proposal for M.S. at University of Vermont).

Nelson, G., and J. Geoghegan. 2002. Modeling Deforestation and Land Use Change: Sparse Data Environments. *Agricultural Economics* **27**(3), 201-216.

Porêba , G. 2006. Caesium-137 as a soil erosion tracer: a review. *Geochronometria* **25**, 37-46.

Reiners, P. W., T. A. Ehlers, S. G. Mitchell, and D. R. Montgomery. 2003. Coupled spatial variations in precipitation and long-term erosion rates across the Washington Cascades. *Nature* **426**:645-647.

Pizarro, J., P. M. Vergara, J. L. Morales, J. A. Rodriguez, and I. Vila. 2014. Influence of land use and climate on the load of suspended soilds in catchments of Andean rivers. *Environmental Monitoring and Assessment* **186**(2):835-843.

Sahin, V., and M. J. Hall. 1996. The effects of afforestation and deforestation on water yields. *Journal of Hydrology* **178**(1): 293-309.

Schmidt, A. H., D. R. Montgomery, K. W. Huntington, and C. Liang. 2011. The question of Communist land degradation: new evidence from local erosion and basin-wide sediment yield in SW China and SE Tibet. *Annals of the Association of American Geographers* **101**(3)**,** 1-19.

Shapiro, J. 2001. *Mao's War Against Nature: Politics and the Environment in Revolutionary China.* Cambridge, UK: Cambridge University Press, Print.

Song, C., and Y. Zhang. 2010. Forest cover in China from 1949 to 2006. In: Nagendra, H., Southworth,J.(Eds.), *Reforesting Landscapes*. Springer, Dordrecht, pp.341–356.

Stokes, S., and D. E. Walling. 2003. Radiogenic and isotopic methods for the direct dating of fluvial sediments. In *Tools in Fluvial Geomorphology*. Ed. Kondolf, G. M., and H. Piégay. Hoboken, NJ: Wiley. Pp. 233-267.

Trac, C.J., Harrell, S., Hinckley, T. M., and Henck, A.C. 2007. Reforestation programs in Southwest China: Reported success, observed failure, and the reasons why. *Journal of Mountain Science* **4**(4), 275-292.

Urgenson, L., A. H. Schmidt, J. Combs, S. Harrel, T. Hinckley, Q. Yang, Z. Ma, Y. Li, H. Lü, and A. Maclver. 2014. Traditional livelihoods, conservation and meadow ecology in Jiuzhaigou National Park, Sichuan, China. *Human Ecology* **???**

U.S. Geological Survey (USGS). 2008. Eurasia land cover characteristics data base version 2.0. In *Global land cover characterization*, ed. USGS. Reston, VA: USGS. http://edc2.usgs.gov/glcc/euras_int.php (last accessed 7 September 2013).

U.S. Geological Survey (USGS). Declassified Satellite Imagery – 1. https://lta.cr.usgs.gov/declass_1 (last accessed 10 March 2014).

U.S. Geological Survey (USGS). Landsat Multispectral Scanner (MSS). https://lta.cr.usgs.gov/MSS (last accessed 10 March 2014).

U.S. Geological Survey (USGS). Landsat Thematic Mapper (TM). https://lta.cr.usgs.gov/TM (last accessed 10 March 2014).

Walling, D. E., and J. C. Woodward. 1992. Use of radiometric fingerprints to derive information on suspended sediment sources. *Erosion and Sediment Transport Monitoring Programmes in River Basins* **210**: 153-163.

Walling, D.E., and B.W. Webb. 1996. F. *Erosion and Sediment Yield: Global and Regional Perspectives* (Proceedings of the Exeter Symposium, July 1996.

Weixi County. 2012. "Wei Xi Gai Lan." http://www.weixi.gov.cn/Category_16/Index.aspx Last accessed: April 29, 2014.

Wilson, L. 1973. Variation in mean annual sediment yield as a function of mean annual precipitation. *American Journal of Science* **273**, 335-349.

Xu, J.X., and D.S. Cheng. 2002. Relation between erosion and sedimentation zones in the Yellow River, China. *Geomorphology* **48**, 365-382.

Xu, J., E. T. Ma, D. Tashi, Y. Fu, Z. Lu, and D. Melick. 2005. Integrating sacred knowledge for conservation: cultures and landscapes in southwest China. *Ecology and Society* **10**(2): 7.

Yatagai, A., K. Kamiguchi, O. Arakawa, A. Hamada, N. Yasutomi and A. Kitoh. 2012. APHRODITE: constructing a long-term daily gridded precipitation dataset for Asia based on a dense network of rain gauges. *Bulletin of the American Meteorological Society* **93**, 1401–1415.

Yin, H. F., and Li, C. G. 2001. Human impact on floods and flood disasters on the Yangtze River. *Geomorphology* **41**(2-3)**,**105-109.

Yin., Z.D., C.Q. Zuo, and L. Ma. 2011. T Soil Erosion Features by Land Use and Land Cover in Hilly Agricultural Watersheds in Central Sichuan Province, China. *Computer and Computing Technologies in Agriculture IV* **345**: 538-550.

Zhang, X. B., and A. B. Wen. 2004. Current changes of sediment yields in the upper Yangtze River and its two biggest tributaries, China. *Global and Planetary Change* **41**(3-4): 221-227.

Zhang, Q., C. Xu, S. Becker, and T. Jiang. 2006. Sediment and runoff changes in the Yangtze River basin during past 50 years. *Journal of Hydrology* **331**:511-523.

Figures

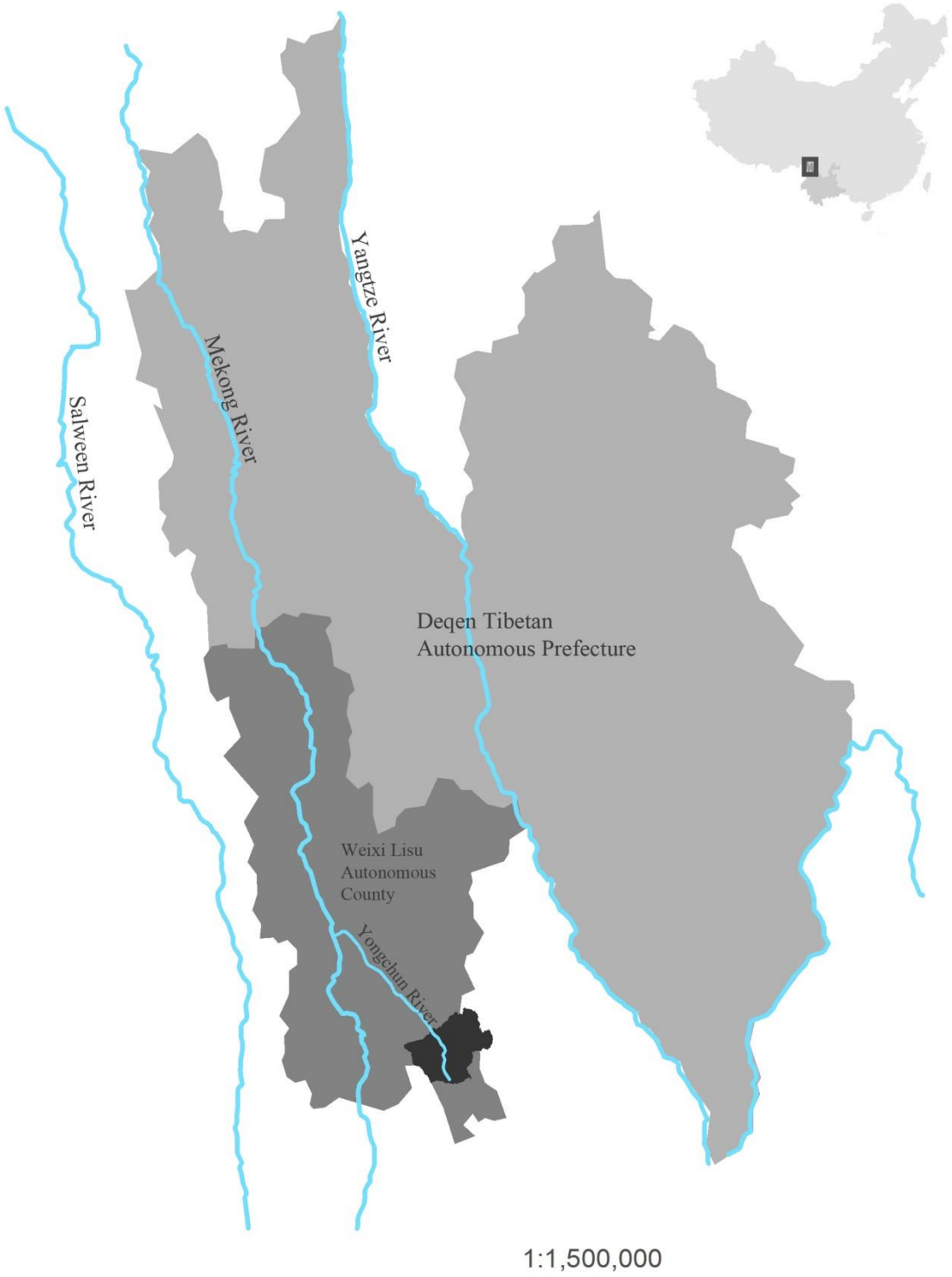

Figure 1. Administrative map of Deqen Tibetan Autonomous Prefecture and Weixi Lisu autonomous County.Yongchuan River is the northwestern flowing tributary that drains the Weixi basin and joins the mainstem Mekong River.

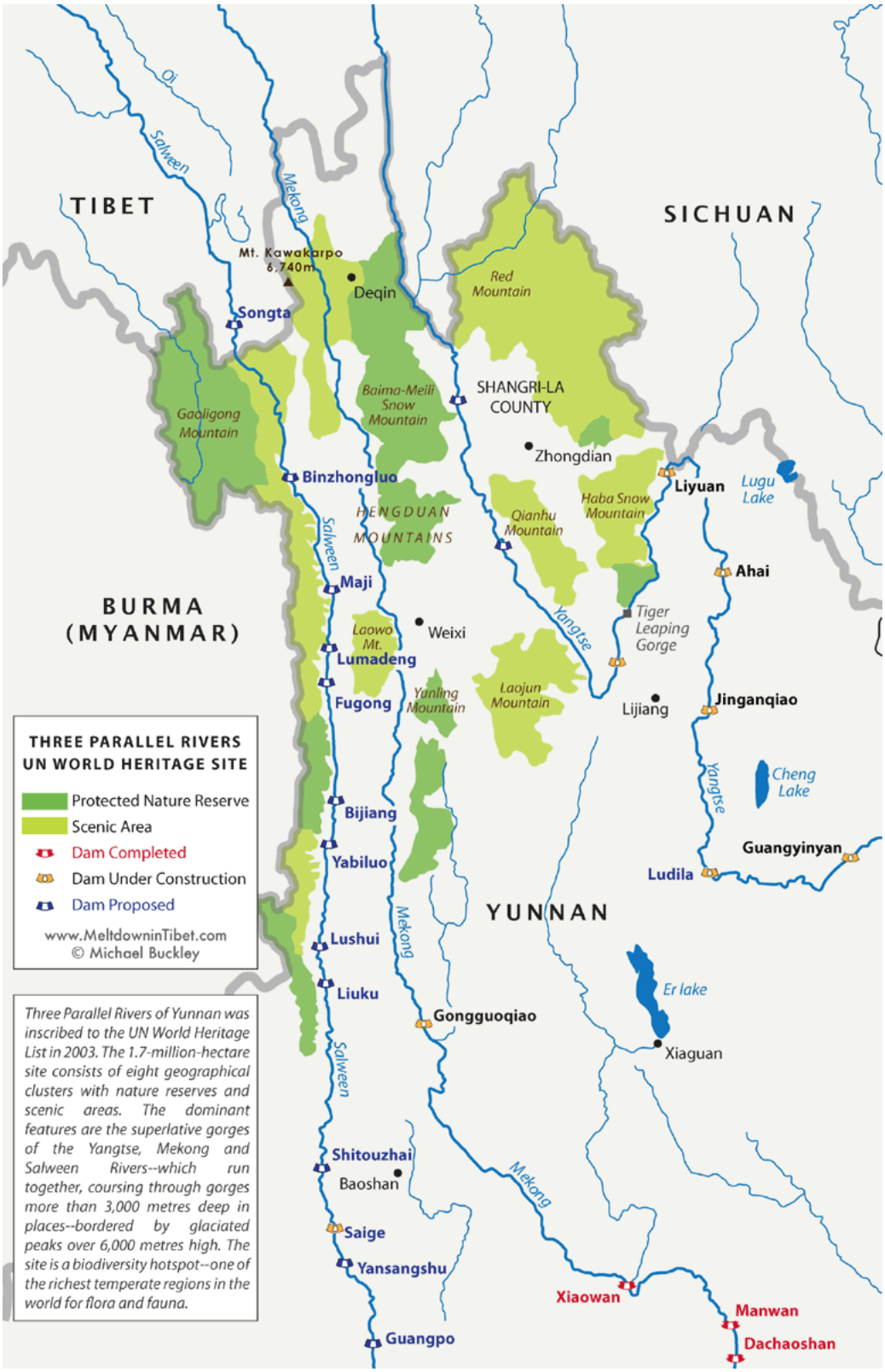

Figure 2. Map of Three Parallel Rivers UN World Heritage Site designation. (Buckley, 2011)

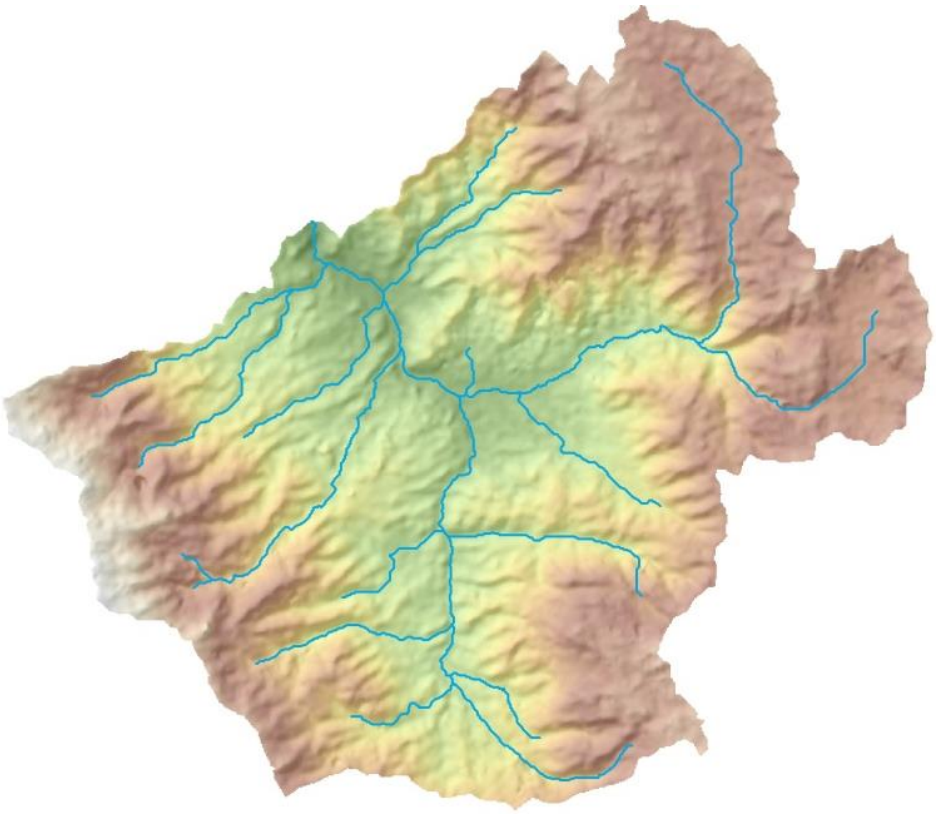

Figure 3. Weixi basin. Different colors show the elevation of the watershed.

Figure 4. Pictures of the hydrology station at the outlet of the watershed and a close-up at the flow meter.

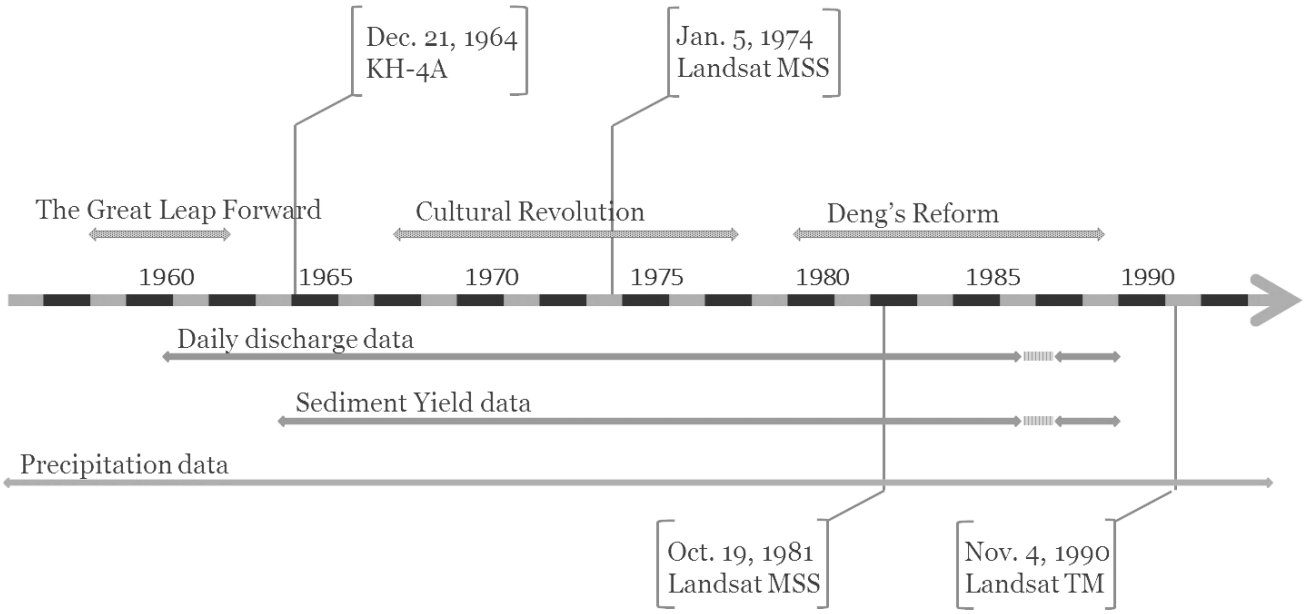

Figure 5. Data used in this project and relevant historical events

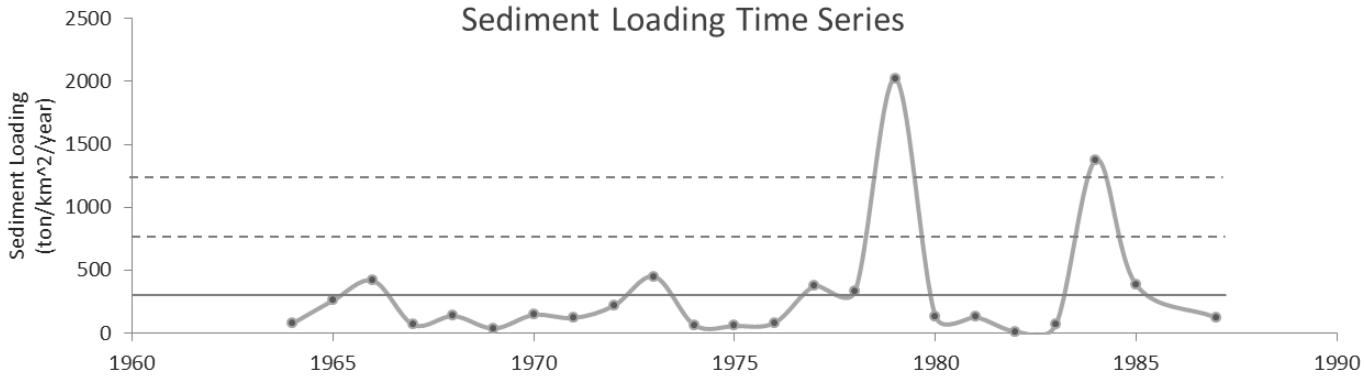

Figure 6. Time series of annual sediment loading between 1964 and 1987. Average is shown in solid line. Dashed lines show one and two standard deviation above the mean.

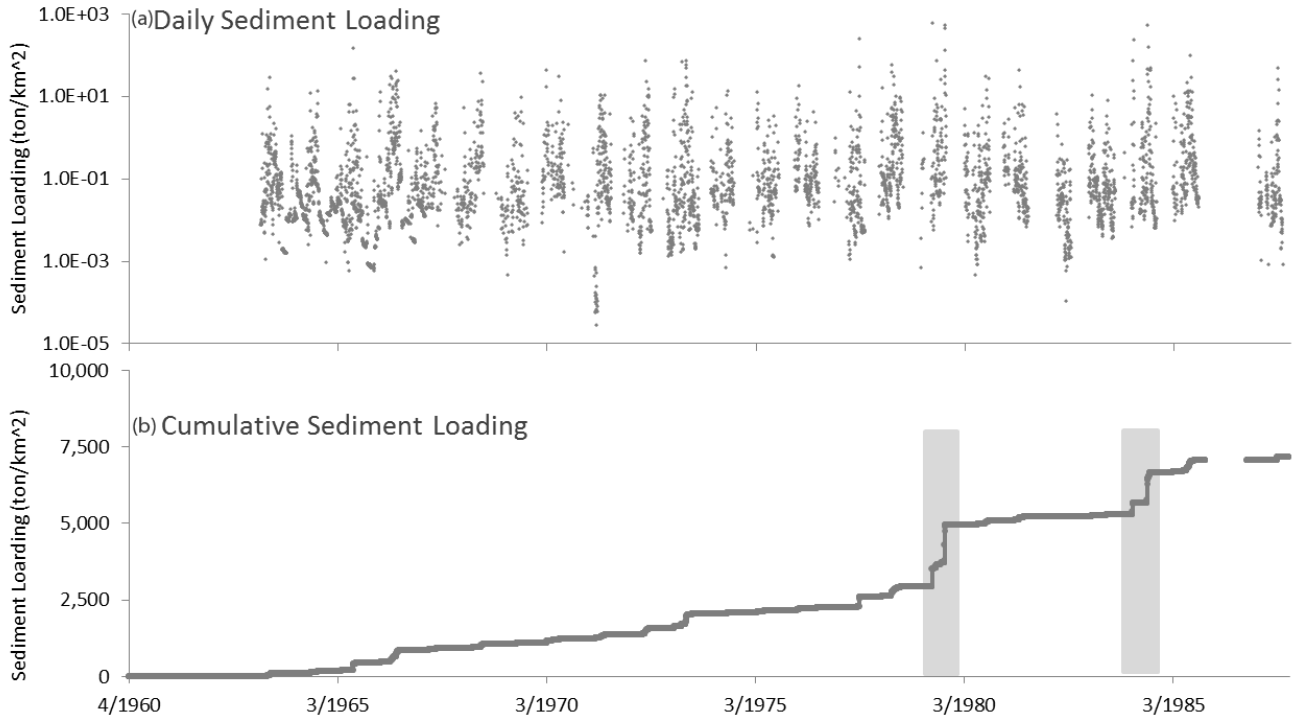

Figure 7. Sediment loading based on daily data. (a) daily sediment loading time series: the scattering of data points does not show any patterns. (b) cumulative sediment loading: a step pattern with relatively low angle slope for most months and abrupt increase in slope for the monsoon season. Two biggest steps occurred in 1979 and 1984, shown in gray bars.

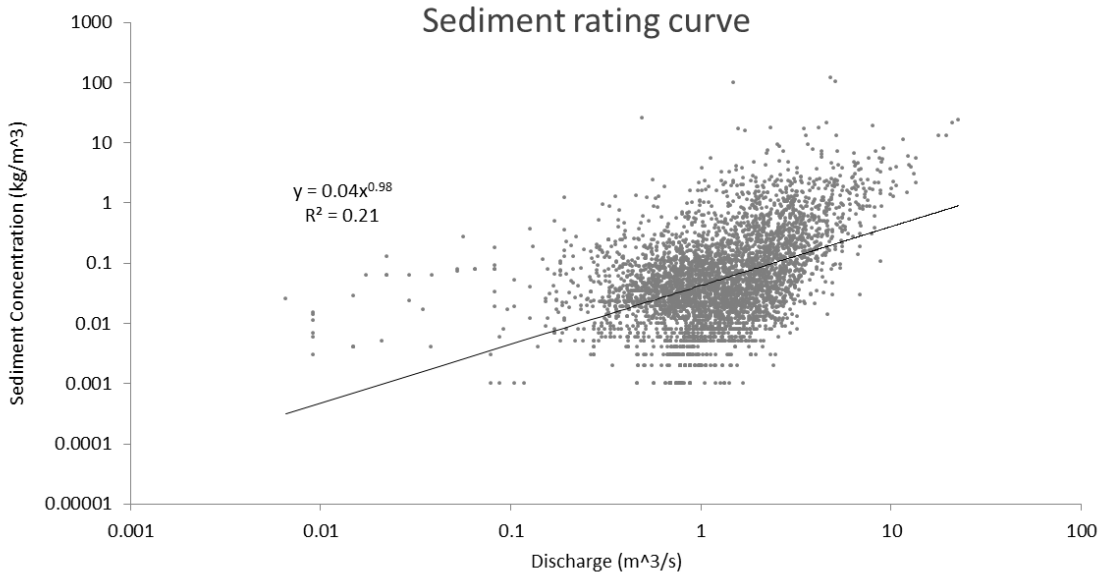

Figure 8. Sediment rating curve of all data points between 1964 and 1987. A general hysteresis effect is observed in this figure. The loop shown in the graph might be seasonal difference in the amount of sediment available to be transporter in the channel.

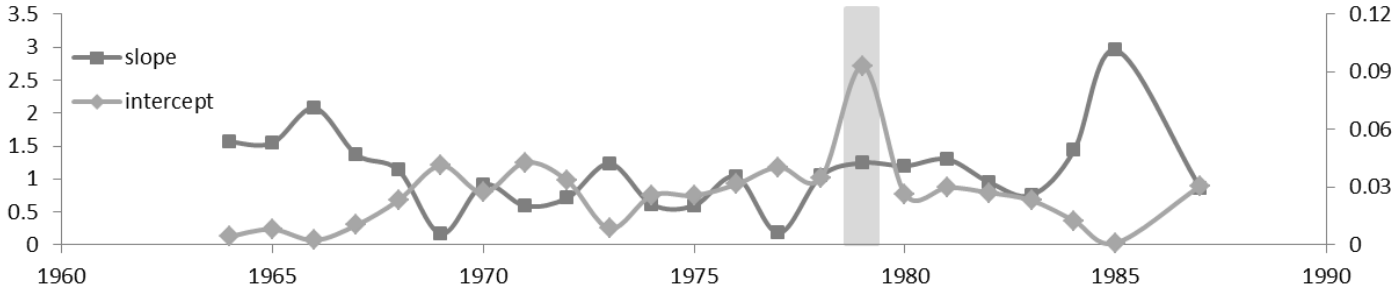

Figure 9. Time series of the sediment rating curve parameter. There is an inverse correlation between slope and intercept. One exception is in 1979, shown in a gray bar.

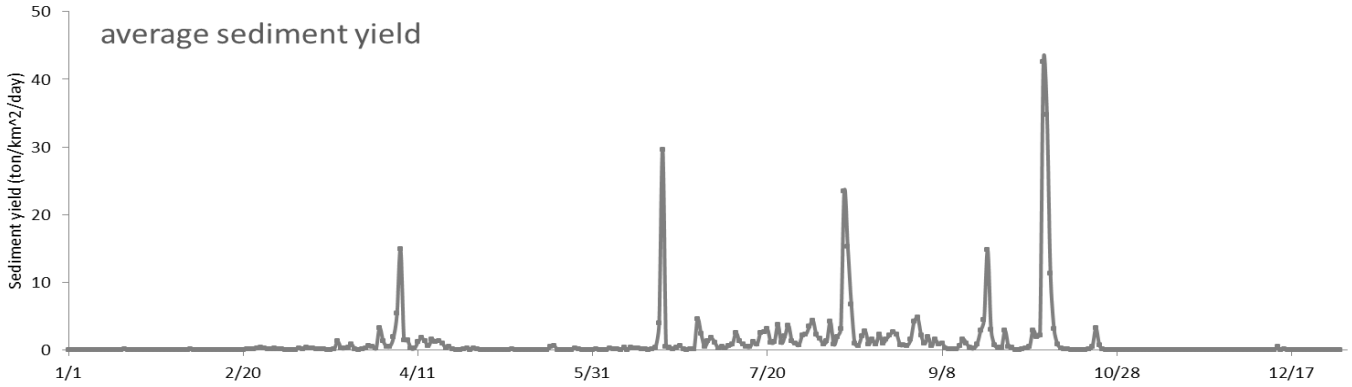

Figure 10. Representative seasonal variation in sediment yield. Each data point is averaged between 23 years of record.

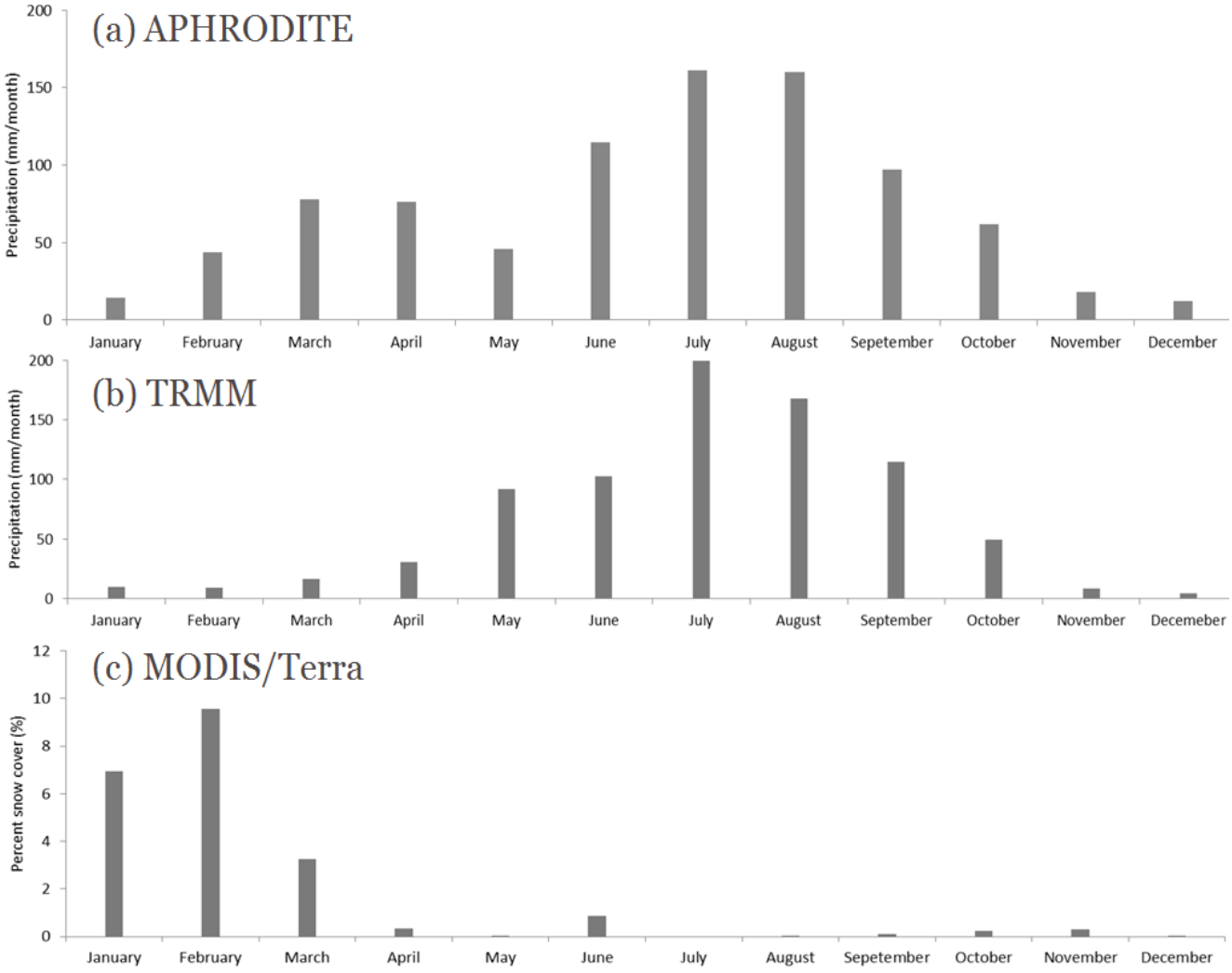

Figure 11. Monthly average of precipitation and percent Snow Cover using three different datasets. APHRODITE shows two distinct peaks, one in the spring and one during the monsoon season. TRMM shows only one peak during monsoon. Combined with the MODIS snow cover data, it is clear that APHRODITE is confusing snowmelt with precipitation in the spring in Weixi basin.

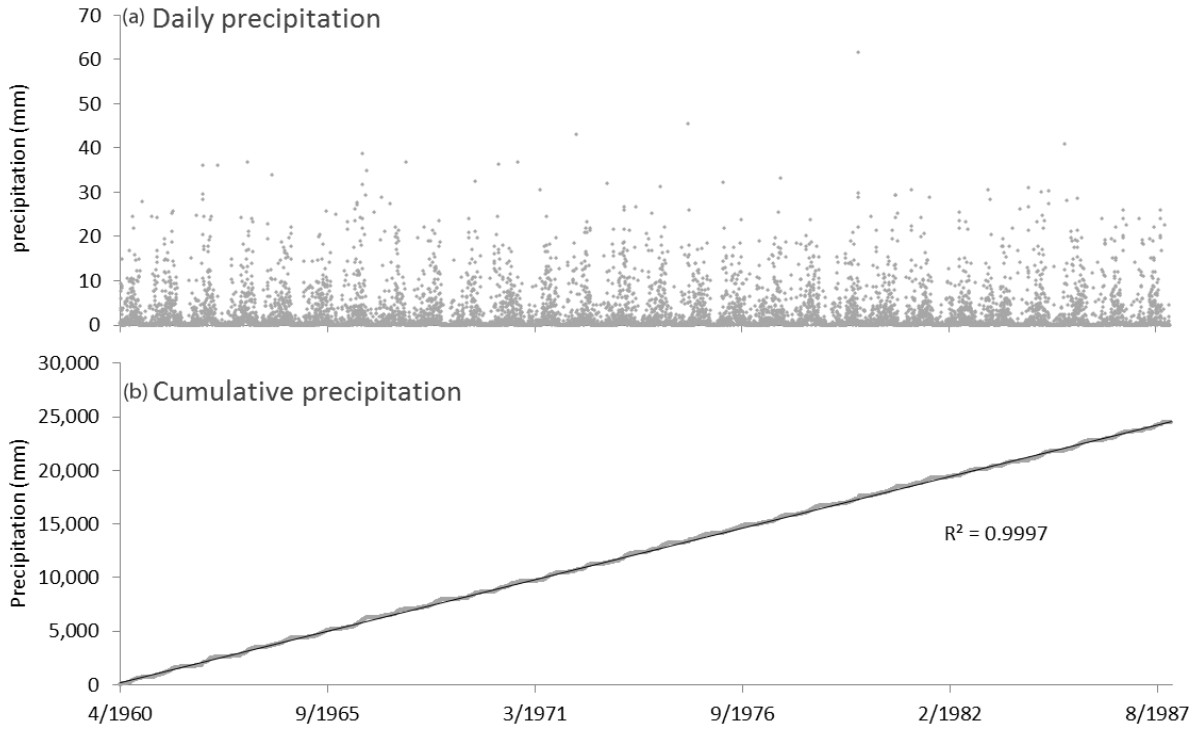

Figure 12. Precipitation. (a) daily precipitation. (b) cumulative precipitation.

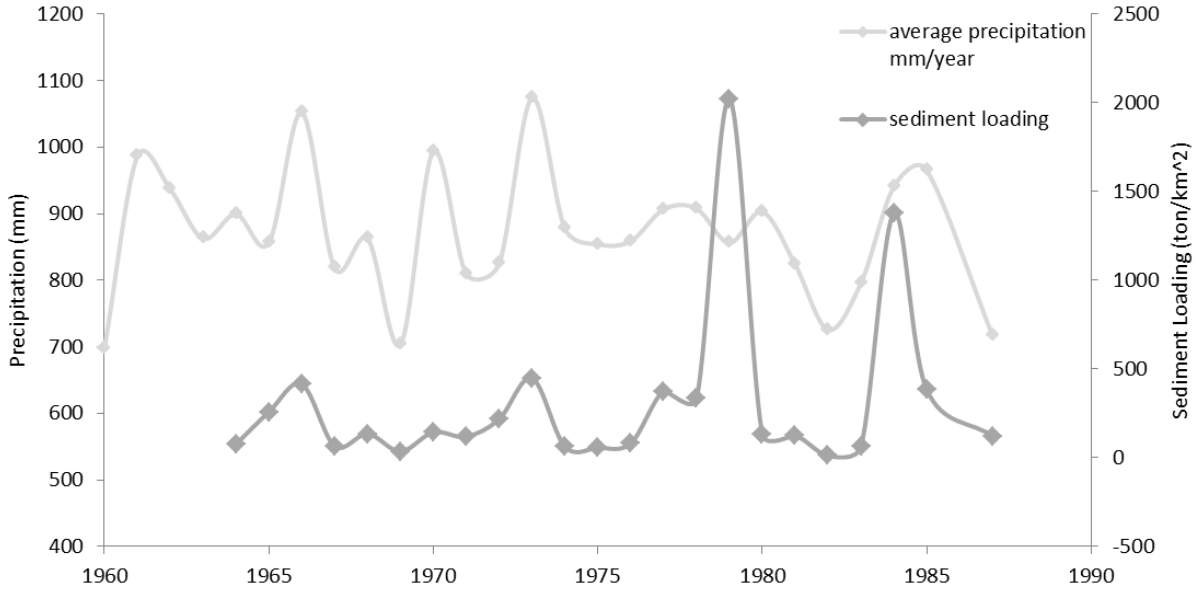

Figure 13. Sediment load co-varies with precipitation except in 1979 and 1984. There is a general trend of higher sediment load corresponding to higher precipitation

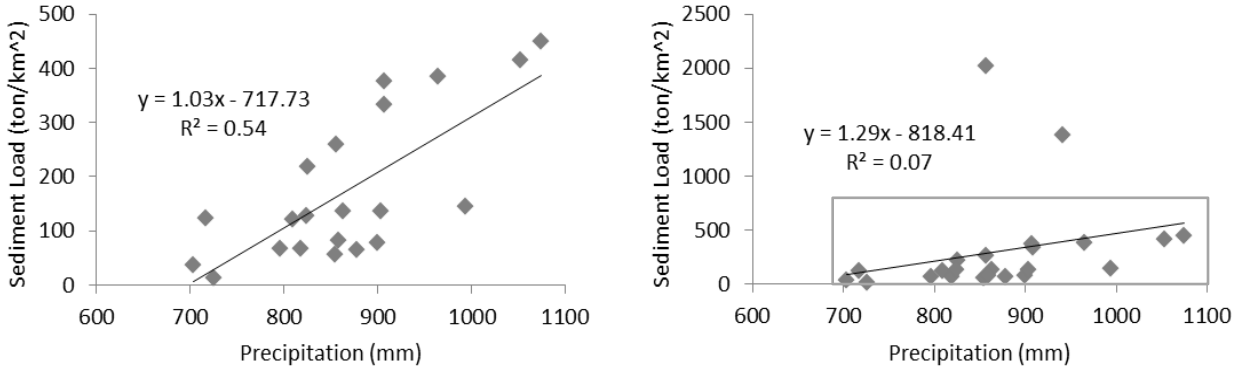

Figure 14. When taking 1979 and 1984 out of the equation, the R^2 value for the correlation between rainfall and sediment load increases from 0.07 to 0.54

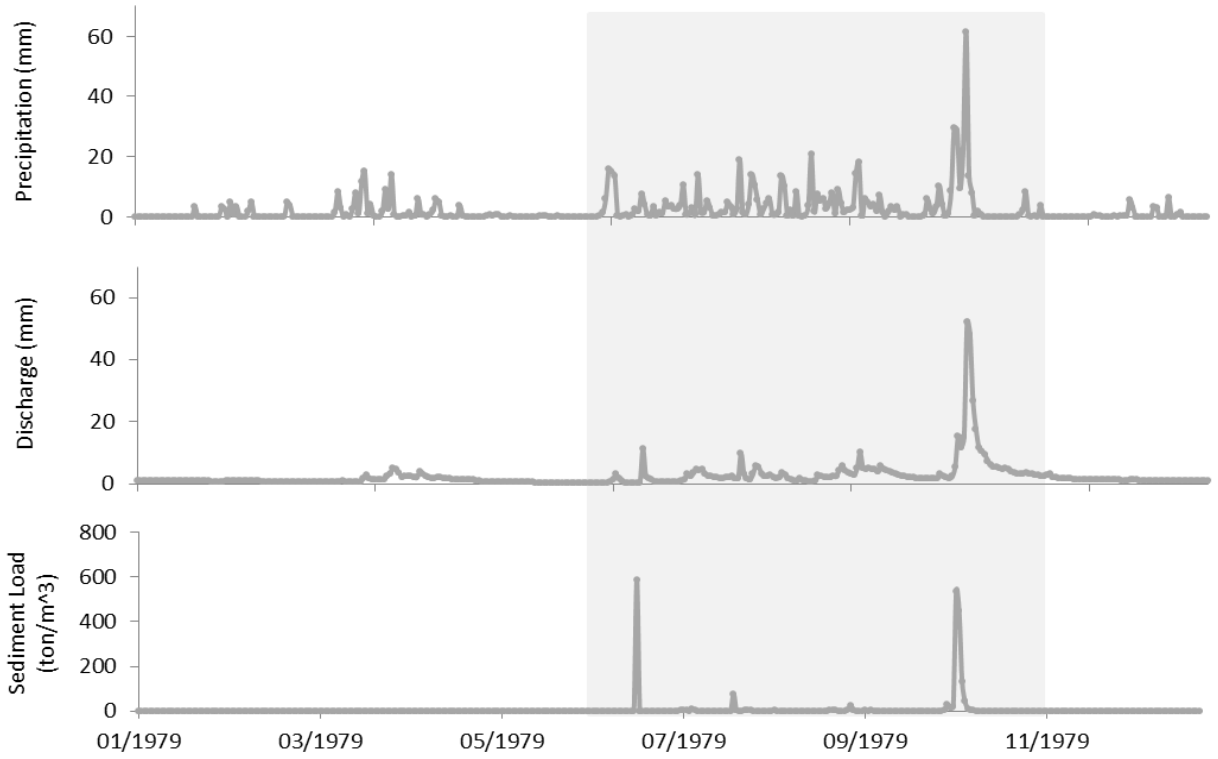

Figure 15. Precipitation, discharge, and sediment load in 1979. Monsoon season is shown in gray background.

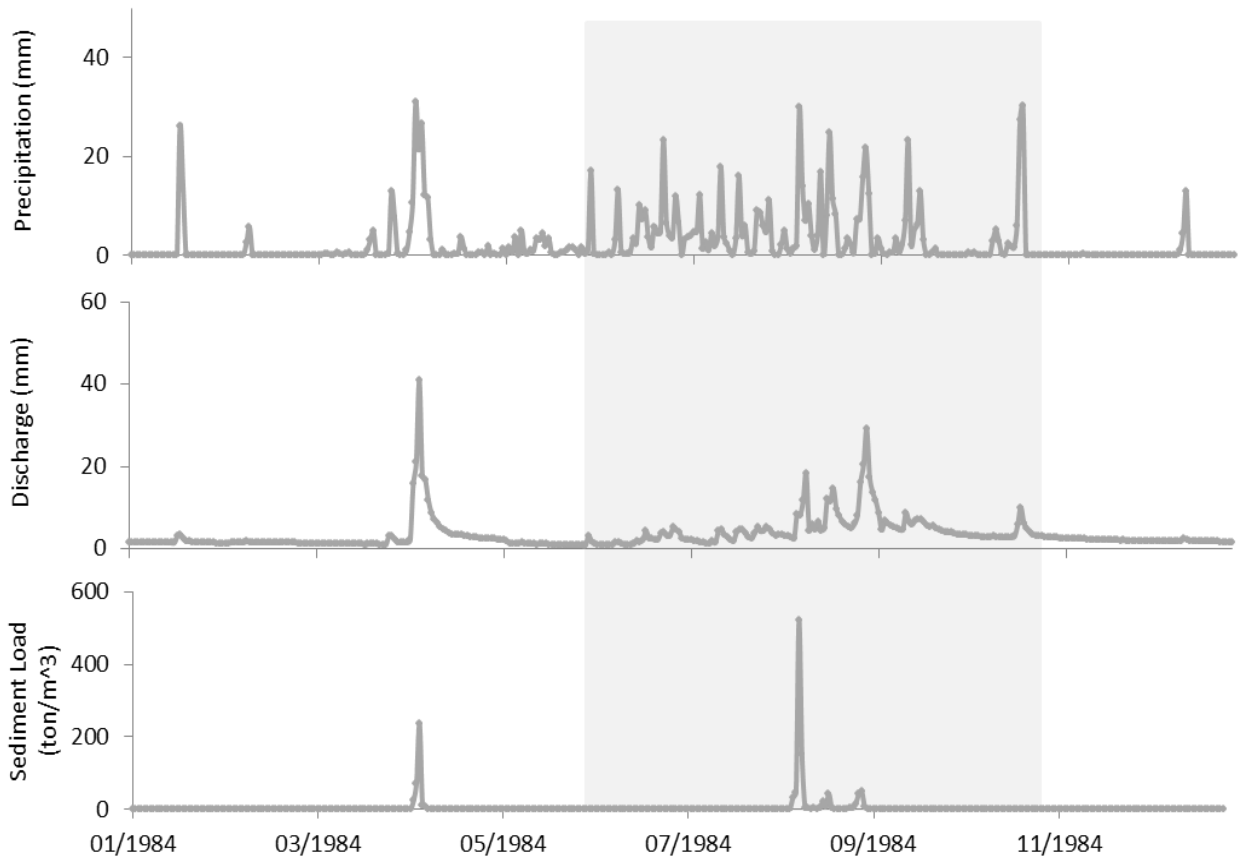

Figure 16. Precipitation, discharge, and sediment load in 1984. Monsoon season is shown in gray background.

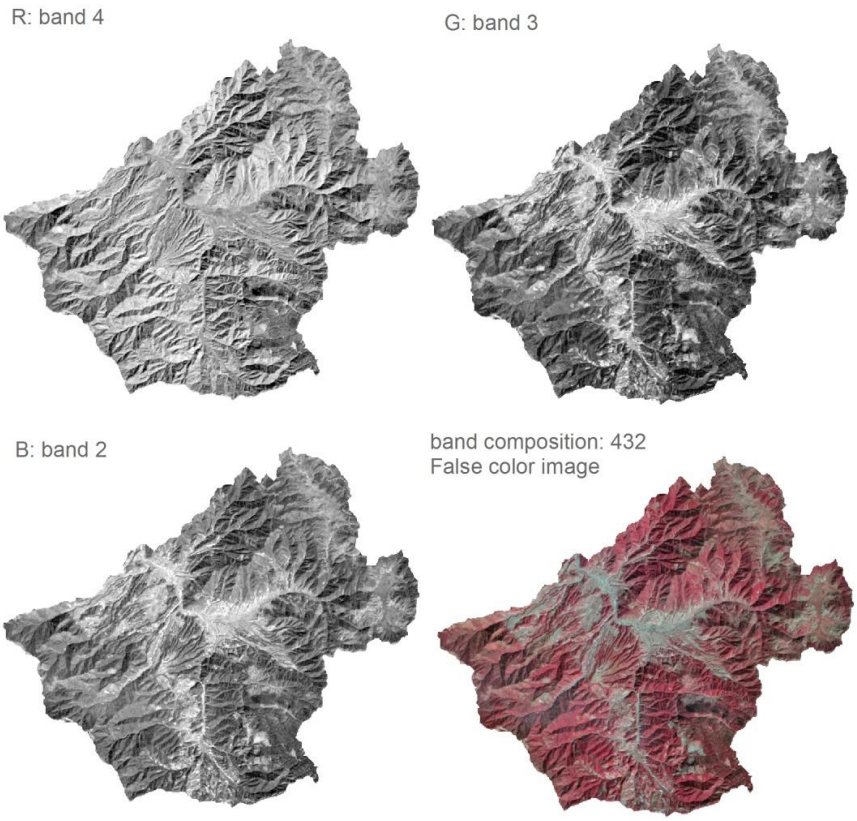

Figure 17. Example of false color band composition from Landsat imagery. 1990 Landsat TM. In the false color image, dark red color shows healthy vegetation whereas blue-white pixels are cleared land or waterway.

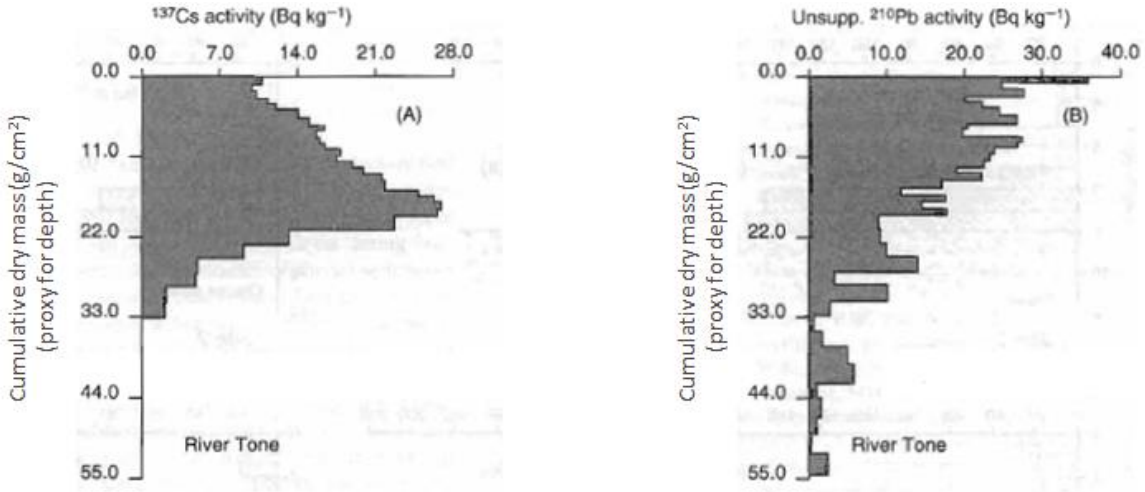

Figure 18. Depth profile of Cs and Pb. Adapted from Stokes and Walling (2003) p.247

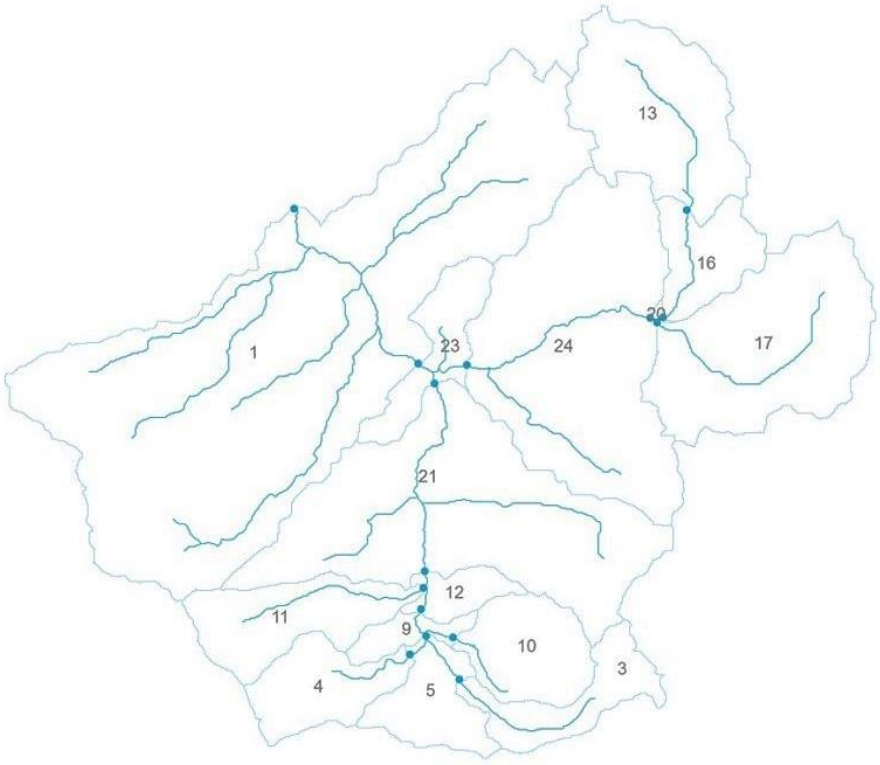

Figure 19. Sample locations.

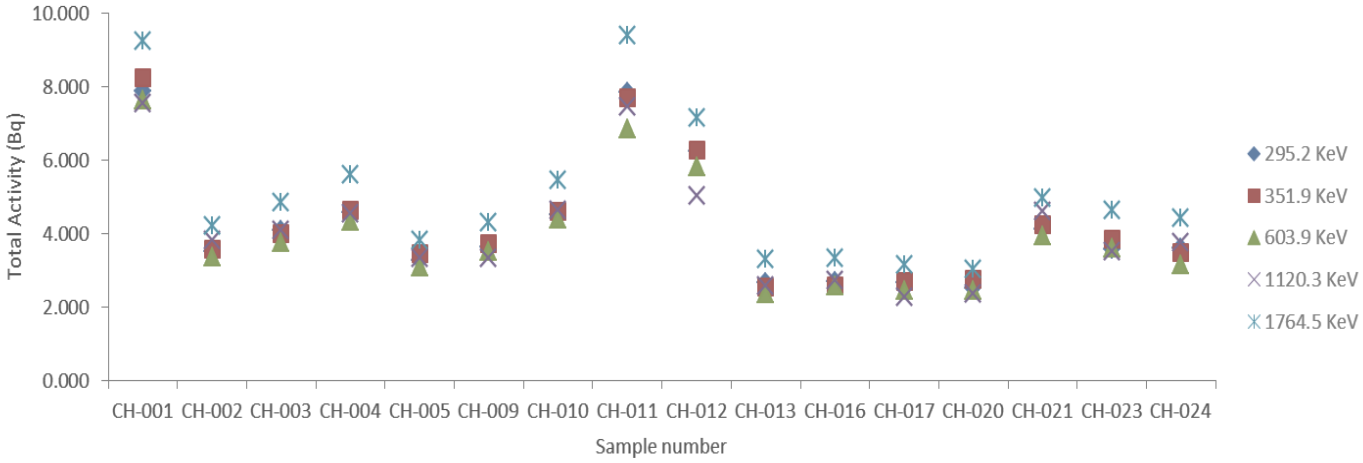

Figure 20. Proxies for ^{214}Pb including ^{214}Pb at 295.2 keV and 351.9 keV, ^{214}Bi at 609.3 keV and 1120.3 keV. ^{214}Bi at 1764.5 KeV is another proxy for supported ^{210}Pb, but it is excluded from the calculation as its activity is unexpectedly higher than the other four proxies for all samples.

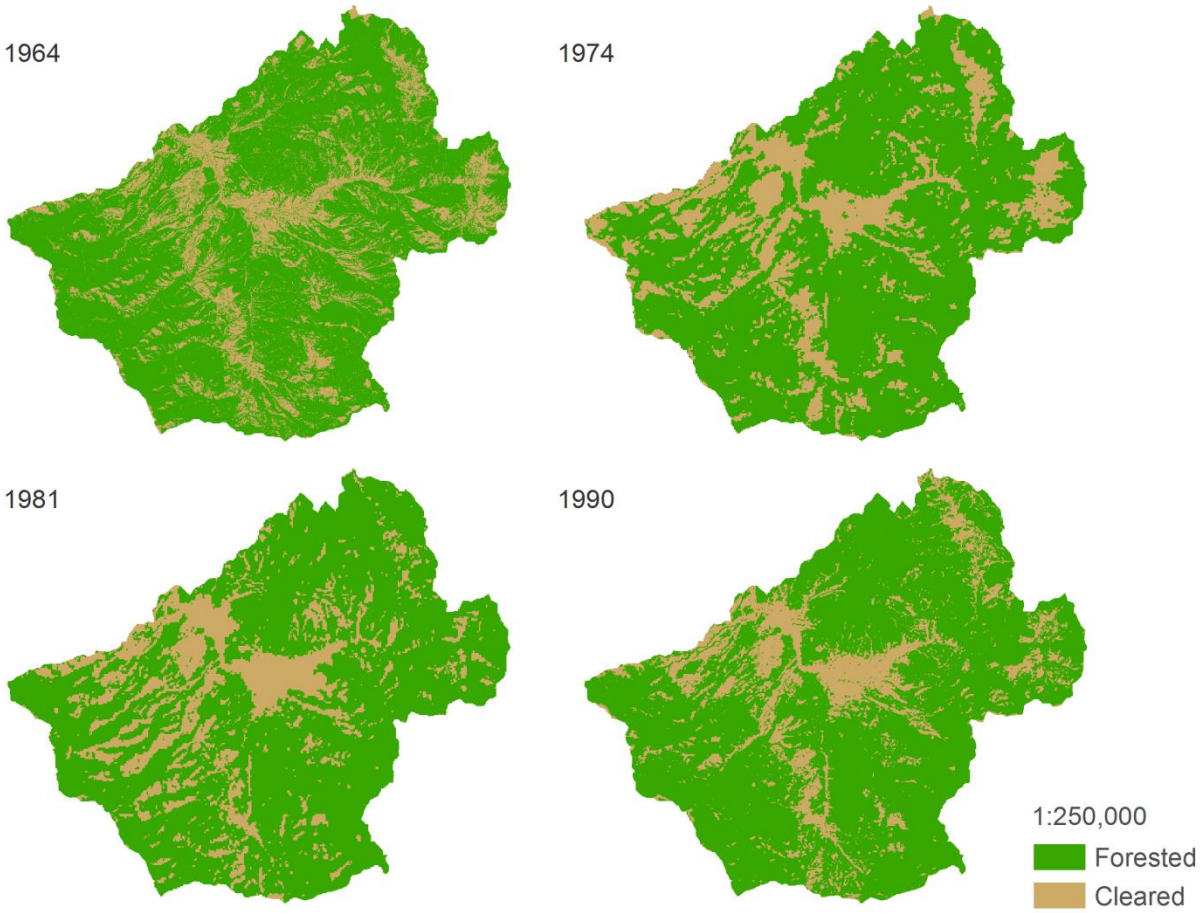

Figure 21. Land cover map of 1964, 1974, 1981 and 1990. Green is forested land and tan is cleared land.

Figure 22. Example of panchromatic image from declassified Keyhole-4A satellite.

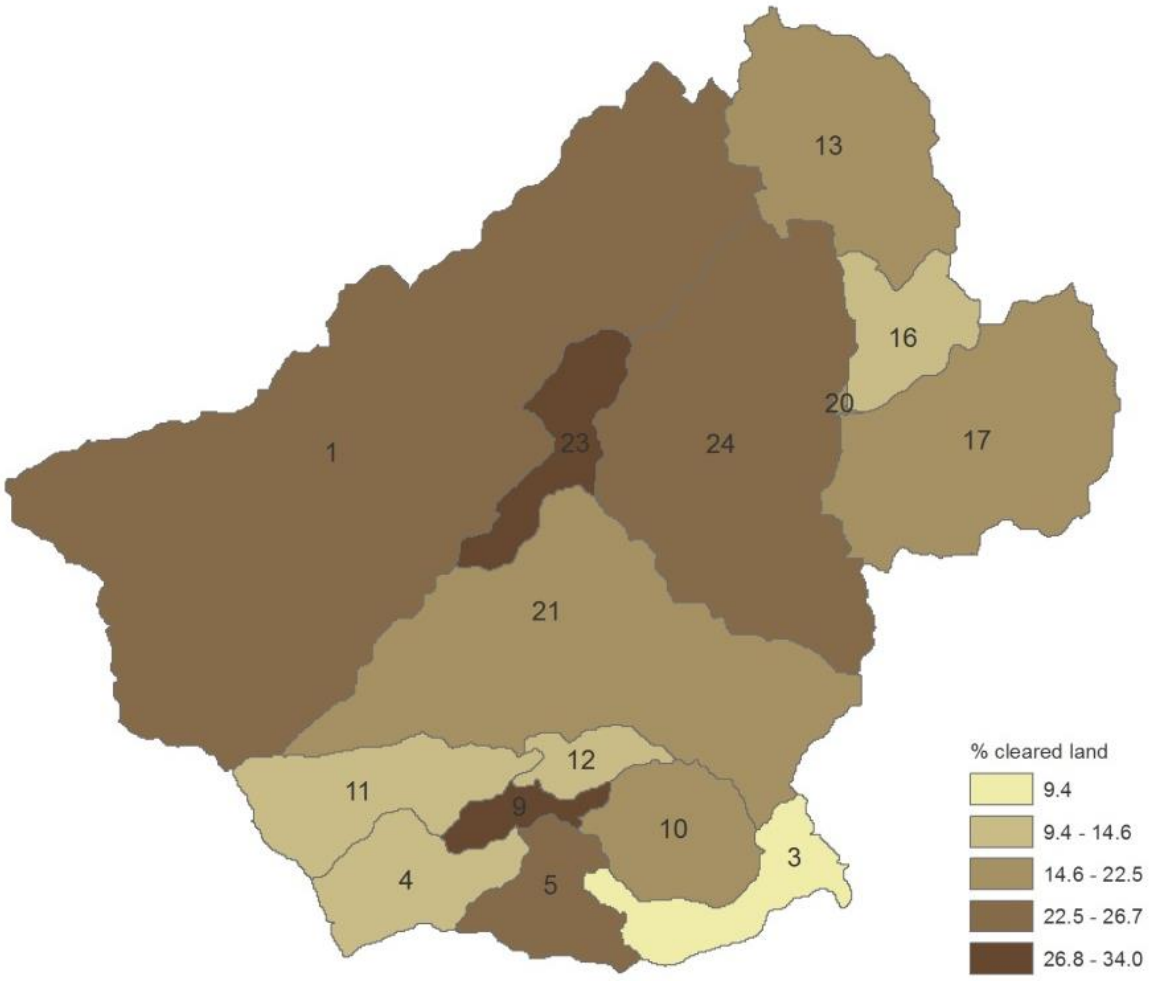

Figure 23. % cleared land for all sub-watershed. Number is averaged between the four years with data.

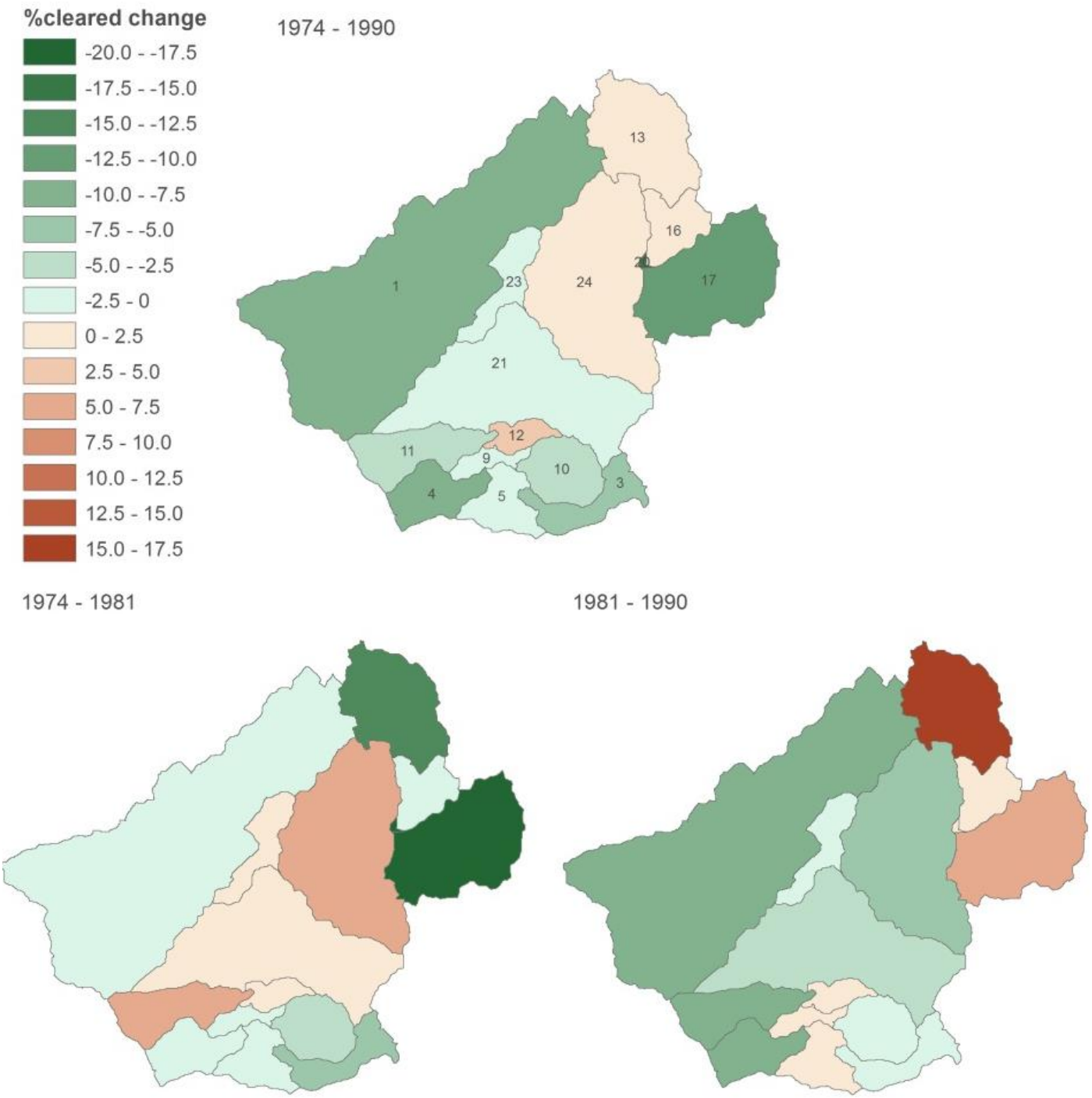

Figure 24. Change of % cleared land on a sub-watershed scale between 1974 and 1990. Changes are further divided into two period: 1974-1981 and 1981-1990. Sub-watersheds with a net increase in % land clearing are shown in shades of red; whereas those with a net decrease in land clearing are shown in shades of green.

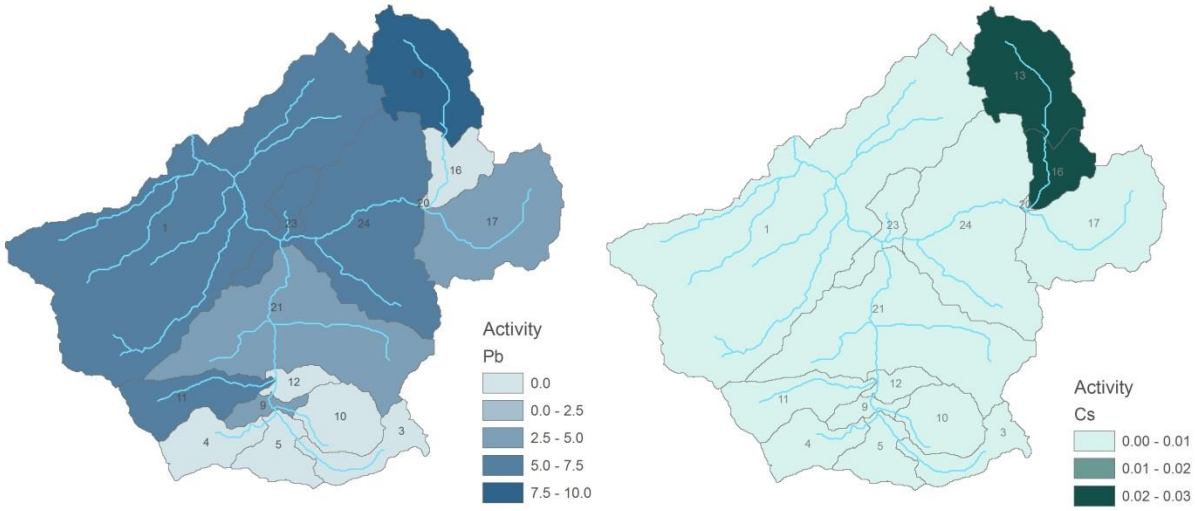

Figure 25. Activity of unsupported ^{210}Pb and ^{137}Cs by sub-watersheds.

Figure 26. Field picture of sub-watershed 13 and 16.